SMARTPHONE POWER CONSUMPTION CHARACTERIZATION AND DYNAMIC OPTIMIZATION TECHNIQUES FOR OLED DISPLAY

by

Xiang Chen

B.S. in Automation,

Northeastern University, China, 2010

M.S. in Electrical Engineering,

University of Pittsburgh, 2012

Submitted to the Graduate Faculty of

the Swanson School of Engineering in partial fulfillment

of the requirements for the degree of

Doctor of Philosophy

University of Pittsburgh

2016

UNIVERSITY OF PITTSBURGH

SWANSON SCHOOL OF ENGINEERING

This dissertation was presented

by

Xiang Chen

It was defended on

May 23rd, 2016

and approved by

Yiran Chen, Ph.D., Associate Professor, Department of Electrical and Computer Engineering

Mingui Sun, Ph.D., Professor, Department of Neurological Surgery

Ervin Sejdic, Ph.D., Assistant Professor, Department of Electrical and Computer Engineering

Zhi-Hong Mao, Ph.D., Associate Professor, Department of Electrical and Computer Engineering

Gregory F. Reed, Ph.D., Professor, Department of Electrical and Computer Engineering

Dissertation Director: Yiran Chen, Ph.D., Associate Professor, Department of Electrical and Computer Engineering

SMARTPHONE POWER CONSUMPTION CHARACTERIZATION AND DYNAMIC OPTIMIZATION TECHNIQUES FOR OLED DISPLAY

Xiang Chen, PhD

University of Pittsburgh, 2016

Smartphones have emerged as the most popular and frequently used platform for the consumption of multimedia. Following the rapid growth of application number and the explosion of cellular network bandwidth, high power consumption, and limited battery capacity remain as the major challenges in smartphone designs. Therefore, lots of research is made to characterize and optimize the smartphone power performance.

However, the existing research approaches on smartphone power characterization generally ignore the impact from the components' varying performance in different applications, as well as users' behavior during the practical usage. Hence, the power optimization techniques in the modern smartphone are inflexible to adapt to different application scenarios and user behaviors.

In this dissertation, I first proposed a new smartphone power consumption characterization and analysis approach – "SEER", which was associated with both user ethological and smartphone evolutionary perspectives. The real-time power consumption is measured with a set of the most popular applications on different generations of Samsung Galaxy smartphones. And deep analysis is made to find how each smartphone component is utilized in different applications, and how the users' daily usage patterns impact on final energy consumption. The experiments show that some traditional power-hungry components, such as Wi-Fi and CPU, actually consume much less energy in practical daily usage. Meanwhile, OLED display panel is still the biggest power consumer in the whole smartphone system; even it's considered the most promising low power display technology.

To further optimize the display power consumption with OLED. I further proposed a set of dynamic power optimization techniques for OLED display, balancing the real-time power perfor-

mance and the user visual perception experience. In this dissertation, the optimization is full-filled at three different levels: 1) Hardware based Optimization: Based on the traditional AMOLED display pixel driver, a novel DVS-friendly OLED driver design is proposed, which can minimize the display color distortion under aggressive supply voltage scaling. Correlated fine-grained DVS schemes (DiViCi) are also proposed to utilize the DVS-friendly driver into video streaming applications. 2) Software based Optimization: Despite the hardware modification, a dynamic OLED power model is built to evaluate the OLED panel power consumption and human visual perception quality assessment. A novel video category based dynamic tone mapping (DaTuM) technique is proposed for video streaming; 3) User Interaction based Optimization: The user interaction and visual perception during the display content capture phase are also taken into consideration, a novel OLED power friendly video recording application (MORPh) was also proposed.

Dedicated real-time management and reliability enhancement schemes are explored to promote the applicability of the proposed approaches . Experiments show that, with these power optimization techniques, the OLED display panel power performance on smartphone device is significantly improved with reasonable visual quality controllability.

TABLE OF CONTENTS

LIST OF TABLES

LIST OF FIGURES

PREFACE

This dissertation is submitted in partial fulfillment of the requirements for Xiang Chen's degree of Doctor of Philosophy in Electrical and Computer Engineering. It contains the work done from March 2011 to May 2016. My advisor is Yiran Chen, University of Pittsburgh, 2011 – present.

The work is to the best of my knowledge original, except where acknowledgment and reference are made to the previous work. There is no similar dissertation that has been submitted for any other degree at any other university.

Part of the work has been published in the conferences:

1. **DAC '16**: **X. Chen**, J. Mao, J. Gao, K. Nixon, and Y. Chen. MORPh: Mobile OLED-friendly Recording and Playback System for Low Power Video Streaming The 53^{nd} Design Automation Conference (DAC), to appear, Jun. 2016.

2. **DAC '15**: **X. Chen**, C. J. Xue, and Y. Chen. DaTuM: Dynamic Tone Mapping Technique for OLED Display Power Saving based on Video Classification. The 52^{nd} Design Automation Conference (DAC), Jun. 2015.

3. **HotPower '14**: **X. Chen**, K. W. Nixon, H. Zhou, Y. Liu, and Y. Chen. FingerShadow: An OLED Power Optimization based on Smartphone Touch Interactions. The 6^{th} International Workshop on Power-Aware Computing and System (USENIX HotPower), No. 6, Oct. 2014.

4. **HotPower '14**: K. W. Nixon, **X. Chen**, H. Zhou, Y. Liu, and Y. Chen. Mobile GPU Power Consumption Reduction via Dynamic Resolution and Frame Rate Scaling. The 6^{th} International Workshop on Power-Aware Computing and System (USENIX HotPower), No. 5, Oct. 2014.

5. **DAC '14**: **X. Chen**, M. Dong, C. Zhang, and Y. Chen. Demystify Smartphone Power Consumption: The Evolution of Smartphone Communication Modules. The 51^{st} Design Automation Conference (DAC), Page: 1$\sim$5, Jun. 2014.

6. **CODES+ISSS '13**: M. Zhao, **X. Chen**, Y. Chen, and C. J. Xue. Online OLED Dynamic Voltage Scaling for Video Streaming Applications on Mobile Devices. International Conference on Hardware/Software Codesign and System Synthesis (CODES+ISSS), Page: 1∼10, Oct. 2013.

7. **RTSS '13**: M. Zhao, **X. Chen**, Y. Chen, and C. J. Xue. Online OLED Dynamic Voltage Scaling for Video Streaming Applications on Mobile Devices. Real-Time Systems Symposium (RTSS), Volume 10, Issue 2, Page: 18, Jul. 2013.

8. **DAC-WIP '13**: **X. Chen**, Z. Ma, F. C. A. Fernandes, C. J. Xue, and Y. Chen. Dynamic Tone Mapping on OLED Display Based on Video Classification. The 50^{th} Design Automation Conference (DAC, WIP), Jun. 2013.

9. **HotMobile '13**: **X. Chen**, Y. Chen, Zhan Ma, and Felix C. A. Fernandes. How is Energy Consumed in Smartphone Display Applications? The 16^{th} International Workshop on Mobile Computing Systems and Applications (USENIX HotMobile), No. 3, Feb. 2013.

10. **ASPDAC '13**: K. Nixon, **X. Chen** Z. H. Mao, Y. Chen, and K. Li Mobile User Classification and Authorization based on Gesture Usage Recognition. The 18^{th} Asia and South Pacific Design Automation Conference (ASPDAC), Page: 384∼389, Jan. 2013.

11. **ICCAD '12**: **X. Chen**, C. J. Xue, and Y. Chen. Mobile Devices User – The Subscriber and also the Publisher of Real-Time OLED Display Power Management Plan. The 31^{st} International Conference on Computer-Aided Design (ICCAD), Page: 687∼690, Nov. 2012.

12. **ICCAD '12**: **X. Chen**, B. Liu, M. Zhao, C. J. Xue, X. Guo and Y. Chen. Active Compensation Technique for the Thin-Film Transistor Variations and OLED Aging of Mobile Device Displays. The 31^{st} International Conference on Computer-Aided Design (ICCAD), Page: 516∼522, Nov. 2012.

13. **DAC '12**: **X. Chen**, M. Zhao, J. Zeng, J. Xue, and Y. Chen. Quality-retaining OLED Dynamic Voltage Scaling for Video Streaming Applications on Mobile Devices. The 49^{th} Design Automation Conference (DAC), Page: 1000∼1005, Jun. 2012.

14. **ASPDAC '12**: **X. Chen**, J. Zeng, Y. Chen, and H. Li. Fine-grained Dynamic Voltage Scaling on OLED Display. The 17^{th} Asia and South Pacific Design Automation Conference (ASPDAC), Page: 807∼812, Jan. 2012.

Based on these conference publications, parts of these works have been further improved and submitted in related top-tier journals. Also more journal publications are under work:

1. **X. Chen**, W. Zhang, C. J. Xue, H. Li, and Y. Chen. DiViSi: Quality-retaining Dynamic Driver Voltage Scaling for Organic Light Emitting Diode Displays. IEEE Transactions on Computer-Aided Design of Integrated Circuits and Systems.

2. **X. Chen**, C. J. Xue, X. Guo, and Y. Chen. ACTON: Active Compensation Technique for the Thin-Film Transistor Variations and OLED Aging of OLED Display Panel. IEEE Transactions on Computer-Aided Design of Integrated Circuits and Systems.

ACKNOWLEDGEMENTS

I would like to acknowledge the support of my advisor, Yiran Chen, whose support made this work possible, and to University of Pittsburgh Innovation Program, Pitt Ventures Program, and National Science Foundation Project for directly providing much of the financial support. I'd like to thank Professor Yiran Chen and Professor Hai (Helen) Li for their excellent guidance during the research. Professor Yiran Chen gives me guidance to become a qualified student and helped to me to develop my potential in my future career. Special thanks go to Professor Minggui Sun, Professor Ervin Sejdic, Professor George Reed and Professor Zhi-Hong Mao for being my committee members. I also would like to thank Professor Jason Xue from City University of Hong Kong, for his guidance and encouragement during my Ph.D. study.

Besides, I'd like to express my gratitude to the members from Evolutionary Intelligent (EI) lab at Swanson School of Engineering, especially Kent W. Nixon, Yaojun Zhang, Wujie Wen, and Chenchen Liu for their consistent supports during my research. Finally, I'd like to thank my family in China for their great encouragement during the whole Ph.D. research.

1.0 INTRODUCTION

Following the rapid growth of Apps number and the explosion of cellular network bandwidth, smartphone has become the consumer electronic device having the most interaction with us in daily life. High power consumption and limited battery capacity, however, still remain as the major challenges in smartphone designs. Many studies were conducted to quantitatively characterize the power consumption of each component in smartphones, e.g., display, multimedia processing, wireless communication etc., and explore the relevant power optimization approaches [2, 3]. In general, the existing research of smartphone power analysis can be mainly divided into two categories: 1) component-level study, which often ignores the correlation among the power consumption of the components in running different Apps [4]; and 2) system-level study, which commonly assumes a static power model [5] or focuses on peak power consumption [6]. However, with these approaches, the smartphone power still lacks of sufficient study, for example: over generations of smartphone evolution, the energy distribution change of different components might remained unknown and some traditional component-level power optimization topic might be trivial to modern smartphones. Also, only assuming a static power model and ignoring the users' smartphone interaction's impact on smartphone consumption, would not lead a practical energy analysis with realistic smartphone usage scenarios.

To tackle these two challenges, I conducted power analysis on the major components of smartphones (i.e., CPU, display, Wi-Fi, GPS, and cellular) from two different aspects:

1) I obtained the power profiling of the smartphones for the selected representative Apps and then compared the power consumption of the different components over four generations of Samsung Galaxy series – from Galaxy S1 to Galaxy S4. Instead of directly measuring the power of the target components, a function-based measurement approach is introduced to decouple the power consumption of different components and derive the components power break-down I need.

2) Based on the characterization results, I am able to combine the practical user smartphone usage traces, to derive the actual energy usage in daily life.

From this evolutionary and ethological smartphone analysis approach, the obtained power consumption trend of the smartphone and each component can help accurately predicting the hot energy dissipation for future smartphone power optimization focus, resulting in a more efficient power optimization flow. Our results show that: different from previous research results [2, 3, 7, 8], the power efficiency of the CPU and radio components keep significant improving over the smartphone generations. However, even all the smartphone devices under test are equipped with OLED display, which is considered as the most promising display technology with excellent power efficiency, the OLED display panels still become bigger and bigger energy consumers.

Display power optimization is always one of the most important topics in mobile device research. Following explosive growth of mobile device shipments, portable display has also experienced several major technology revolutions, such as STN (Super-twisted Nematic), color LCD (Liquid Crystal Display), and the latest OLED (Organic Light Emitting Diode). OLED is one of the most promising display technologies to replace LCD. In an OLED pixel, a set of organic thin films (i.e., three corresponding to the RGB colors), is sandwiched between two layers of conductors. When a current is applied, specific strength of fluorescent light is emitted from the organic thin films. Different colors can be generated by the organic thin films with different dopant. Compared to LCD, the advantages of OLED are: 1) Since OLED pixels can emit light by themselves without backlight panel, the average power efficiency is significantly improved. The power consumption of an OLED panel is generally around 60% of a LCD panel with the same size [9], 2) OLED has much brighter colors and higher contrast ratio, and its displaying quality is not constrained by view angles or temperature [10]; 3) OLED panels can be built on flexible and transparent substrates [11].

Although the power efficiency of OLED has been significantly improved since it was invented, OLED display panel is still one of the major contributors to the overall power consumption of smartphones. This is because the OLED's display power consumption is primarily determined by the displayed color on each pixel. Although the average power consumption of OLED display panel is much lower than the LCD panel, when displaying much brighter or lower power efficient colors, such as pure white and bright blue, the power consumption of OLED might be 3 times of the LCD panel. Unfortunately, for our smartphone usage study, I found that, those lower power

efficient colors are widely adopted in Apps design. For example, in the web browsers, the background color usually adopts white, which has the lowest power efficiency, since all sub-pixels are working on the highest luminance.

To improve the OLED display panel power efficiency, many OLED power optimization approaches have been proposed, such as dynamic voltage scaling (DVS) for static images [12], and color re-mapping in user interface and browsers [13]. Meanwhile, there are also power management methods inherited from LCD technology requiring minimum analysis works, e.g., global luminance dimming and overall color tone tuning [14, 15]. However, these techniques also suffers from two major defeats: 1) Many OLED power management techniques focus on controlling pixel color composition, i.e., remapping the pixel color to the one with lower power consumption. And these techniques generally ignore the display distortions impact on users visual perception and can substantially influence viewer experience [14, 16, 17]. 2) In many power management techniques targeting video streams, the analysis of video content is often required [12, 18]. These video or image pre-analysis workloads will introduce considerable power consumption overhead into a real-time smartphone system and suffer from system resource constrains.

Hence, with a better understanding of the smartphone systems energy distribution and user experience concern, I also put lots of efforts to OLED display panel power optimization. In this research focus, to avoid the overhead related to the content analysis, I propose to extract the common features of specific video categories from the viewpoint of OLED display panel power characteristics and then apply custom-designed optimization policies accordingly. Designated DTM policies are applied to a video stream based on its category and power features. I refer to this technique as video classification based dynamic tone mapping (DaTuM) scheme. Since many DTM algorithms have already been integrated in the display engine of many modern smartphones, the technical barrier of applying DaTuM in real systems is very low and a video player application has been demonstrated accordingly in this work. Experiment results show that proposed DaTuM ensures 17.80% power saving of OLED display panel on average. Further analysis shows that compared to the DTM scheme based on official category information provided by the video streams themselves, the proposed DaTuM scheme offers higher power saving as well as better display quality control.

Moreover, I proposed a set of OLED driver circuit oriented power optimization design to enhance the power efficiency in a hardware perspective. I proposed a DVS-friendly driver, which

has better display quality control under DVS power scaling technique. And I also propose correlated OLED Fine-grained DVS (FDVS) technique for video streaming applications. Compared to the existing works on the DVS power management techniques on LCD or OLED displays, our proposed FDVS technique can reduce the OLED display power consumption by 19.05%∼49.05% while maintaining a high display quality. And the users visual experience remained extremely high.

Based on these research, I combined the smartphone power analysis and optimization work with practical user experience. Different from traditional researches, our works reveal a more realistic energy analysis approach and offer better power optimization with reasonable user experience quality.

The rest of our paper is organized as follows:

- I then present the details and expects implementation of our novel smartphone energy analysis approach, in Chapter 2.
- I show our OLED power optimization work in hardware level with Chapter 3.
- I show our OLED power optimization work in software level with Chapter 4.
- I show our OLED power optimization work in interaction level with Chapter 5.
- Finally I introduce our future work directions - further user interaction based smartphone energy analysis and OLED power optimization work, is shown in Chapter 6.

The proposed work can be decoupled as following two main research scopes: 1) to construct a better smartphone power analysis approach from both user ethological and smartphone evolutionary perspectives, and use it as guidance for smartphone power research; 2) with a better understanding of the smartphone energy distribution and user experience concern, to design a set of dedicated power optimization techniques for OLED display panel, which is the biggest power consumer in smartphones.

For research scope 1, I proposed "SEER", a user ethological study and smartphone evolution based approach, to characterize and analyze the power consumption of smartphone. This approach includes three major tasks: 1) Smartphone components power characterization with different smartphone generations; 2) Smartphone usage study, by examining the open-source smartphone usage data collected through Live-Lab project; 3) Smartphone energy analysis, by combin-

ing the component-level power model and the practical Apps usage patterns. Based on these tasks, our have made the major technical contributions of research scope 1 as following:

- I can reveal the user's smartphone usage behavior patterns and the most preferred Apps in real smartphone usage and categorized them based on their function similarities.
- I can construct a compressive power consumption characterization work flow for major smartphone components, by taking into account the underlining correlation in the identified representative Apps.
- I can establish an ethological analysis approach that is able to construct a near realistic smartphone energy statistics by considering the Apps usage patterns of the users.
- I can establish an evolutionary power consumption trend over four generations of Samsung smartphones, and addressed the most power consuming components in the smartphone analysis.

For research Scope 2, I proposed a set of dynamic power optimization techniques for OLED display panels. Compare to the traditional display power saving technologies, these techniques take the user visual experience into consideration and cover three different layers of smartphone development work: 1) Application level optimization, which is composed of a set of power saving schemes. These schemes can be applied into the smartphone applications with high power saving ratio, low power consumption overhead and reasonable visual quality controllability; 2) Hardware level enhancement, which is supposed to improve the OLED driver power performance with DVS technique; 3) System level management, which explores the management and reliability enhancement schemes to promote the applicability of the proposed techniques.

With these power optimization techniques, the OLED display panel power performance on smartphone device is significantly improved with reasonable visual quality controllability.

Our major technical contributions of research Scope 2 are:

1) In the Hardware Level:

- I can propose a DVS-friendly OLED driver design, that effectively maintains the color accuracy when supply voltage is scaled, as long as the required luminance of the OLED cell is below the driving strength of OLED driver.

- I can quantitatively analyze the relationship between the voltage scaling and the image quality of the OLED displays using conventional and DVS-friendly drivers, respectively, based on human virtual perception index, i.e., Structural Similarity (SSIM).
- I can proposed a fine-grained DVS (FDVS) technique to minimize the OLED power consumption in statistic image and video streaming applications under both spatial and temporal constraints.
- I explored the effectiveness and the cost of pixel color repairing technique to further improve the power consumption and video quality in our proposed OLED FDVS technique.
- I also proposed the peripheral circuit designs for OLED driver circuit reliability enhancements, i.e. process variation and aging effect tolerance.

2) In the Software Level:

- I can improve the dynamic OLED power model, to evaluate the OLED panel power consumption and HVP-quality assessment, which has better accuracy than traditional statistic power model and fits better with video streaming applications.
- I can analyze the power consumption features of several representative video categories and establish a video classifier based on the shared power characteristics of each video category.
- I can develop a set of novel video category based dynamic tone mapping (DaTuM) technique, according to video streams' unique power features to maximize power saving and minimize the impact on visual experience.

3) In the Interaction Level:

- I can explored the management and reliability enhancement schemes to promote the applicability of the proposed techniques from the two levels above.
- I examined the mechanism of one of the most interactive application the now being used in Android system, the video camera.
- I quantitatively examined the camera interaction's impact on the system and display's power consumption.
- I developed a application that utilized the discovered relationship between Android camera and power consumption to save the power during both recording and playback phase.

Also, there are some new ideas to be verified and studied. For the future work directions, I am going to further leverage the user interaction's impact on the practical smartphone power application. And I will focus on the research scope 2 to design dedicated smartphone Apps and system modules for high-reliable and high-performance power optimization. Finally, I will release a set of power-friendly design guidance library for the smartphone to share with power researcher and industry designer.

2.0 SEER: AN ETHOLOGICAL AND EVOLUTIONARY APPROACH FOR SMARTPHONE ENERGY ANALYSIS

In this chapter, I will present the details of the proposed "SEER" - an approach to characterize and analyze the power consumption of smartphones from ethological and evolutionary perspectives. The structure of this chapter is organized as the follows: Section 2.1 gives the background of present smartphone energy and user behavior studies; Section 2.2 presents the details of "SEER"'s analysis methodology and workflow; Section 2.3 presents the evolutionary smartphone components power characterization result. Section 2.4 shows the ethological energy analysis, combing with practical user traces; Section 2.5 presented some preliminary quantitative analysis results on several major smartphone components as case study; Section 2.6 discusses the discovery I drew from "SEER" and talk about the most worthy energy optimization focus on smartphone system.

2.1 SMARTPHONE ANALYSIS BACKGROUND AND RELATED WORKS

2.1.1 Smartphone Power Analysis

The power analysis and optimization of specific single smartphone component have been extensively studied in many prior arts: For example, Balasubramanian and Thiagarajan *et al.* investigated the power consumption of smartphones running network applications in [2] and [3], respectively. In [7], Dogar *et al.* revealed that Wi-Fi module is an significant power consumption source and requires dedicated scheduling optimization. In [8], Liu *et al.* showed that GPS module may consume more than 400mW in some applications. In [13, 19] and [12], Dong has revealed the OLED display panel's power impact in smartphone system. And in [6], Carroll *et al.* built

power models of every smartphone hardware component by leveraging the open source circuit designs. This work give a over view to the static power consumption of each smartphone component. Also, there some works integrated those power models into smartphone system for power monitor and guidance. Some Apps, e.g., AppScope [4] and PowerTutor [5], were developed to perform real-time power measurement of smartphones. Nonetheless, none of the above works consider the correlation among the power consumption of smartphone components in different applications and usage scenarios.

2.1.2 Smartphone User Behavior Analysis

The ethological study of smartphone usage, i.e., the Apps usage pattern, has also become a popular area in mobile system research: In 2006, a team from MIT collected and analyzed the operation tracks of 100 Nokia phone users for one year [20]. In 2010, Falaki *et al.* studied the variability of Android and Windows Mobile smartphone usage among 33 participants in 7$\sim$21 weeks [21]. Very recently, Rice University launched a project named "LiveLab", which systematically collected the smartphone user application trace under different scenarios, including the data of 10 college students on Windows phone for 4 months [22] and 24 university students on iPhone for 1 year [23] etc. Instead of collecting the similar Apps usage trace by ourselves, in this work, I mainly utilize the data set published in [23] to conduct the relevant ethological analysis on smartphone power consumption.

2.2 SEER METHODOLOGY

The foundation of our proposed SEER approach includes three components: 1) the smartphone components power measurement and modeling across smartphone evolutionary generations, considering their usage correlation for different Apps; 2) the ethological analysis on practical users' Apps usage traces; and 3) the energy analysis combining the evolutionary and ethological analysis to reveal the realistic energy consumption.

2.2.1 Smartphone Component Analysis

I selected four generations of Samsung Galaxy S series – Galaxy S1, S2, S3 and S4, which dominated the Android smartphones between 2010 and 2013 [24]. From S1 to S4, the operating system is improved and the hardware became more and more complex and powerful. Table 1 compared the major software and hardware changes of the 4 generations of Samsung Galaxy S series.

Table 1: Smartphone Specifications

	Galaxy S1	Galaxy S2	Galaxy S3	Galaxy S4
OS	Android 2.1	Android 2.3	Android 4.0	Android 4.2
SoC	Exynos 3	Exynos 4	SnapdragonS4	Snapdragon600
CPU	Single-Core 1.0 GHz	Dual-Core 1.2 GHz	Dual-Core 1.5 GHz	Quad-Core 1.9 GHz
GPU	PowerVR SGX 540	ARM Mali 400MP	Qualcomm Adreno 255	Qualcomm Adreno 320
RAM	512 MB	1 GB	2 GB	
Screen	4.0 ” Super AMOLED	4.3” Super AMOLED+	4.8” Super AMOLED HD	5” Super AMOLED HD
Res.	4.0” 800×480	4.3” 800×480	4.8” 1280×720	5” 1920×1080
Wifi	Broadcom BCM 4329	Broadcom BCM 4329	Broadcom BCM 4334	Broadcom BCM 4335
Cellular	SMARTi & Tritium	SMARTi & X-Gold	SMARTi & X-Gold	Broadcom BCM 4335
Network	AT&T 2G	AT&T 3G	AT&T 3G/4G	AT&T 4G
Battery	Li-po 1500 mAh	Li-Ion 1650 mAh	Li-Ion 2100 mAh	Li-Ion 2600 mAh

As presented above, many prior-arts explicitly characterize the power of each smartphone hardware component through circuit or behavior models [2, 6, 3]. These approaches generally ignores the dynamic functional and power correlation among the components under different applications. Moreover, they are often device specific and hard to be extended to more generic smartphone platforms. Hence, in this work, I treat the smartphone as a black box and assume its power is contributed by several major “functional components”, such as *display*, *Wi-Fi* and *Cellular(3G/4G)*. Considering the difference of the components involved, the measurement flow for various Apps is slightly altered to capture the corresponding power breakdown of the smartphone.

The smartphone power is measured by Monsoon power monitor from battery end. During the power measurement, all the smartphones are using their native versions of Android operation system (OS). Hence, the impact of the OS variance is characterized as part of the power consumption difference of the hardware modules. All unnecessary background Apps are turned on during the testing and unrelated notification push services are closed. Since the power consumptions of radio

Figure 1: Smartphone power measurement Setup.

components are significantly influenced by signal strength, all cellular and Wi-Fi related measurements were conducted in open field and our in-house radio lab isolated from signal interference, respectively.

2.2.2 Smartphone User Trace Analysis

I adopted the open-source user application traces collected in LiveLab project [23] in our ethological analysis. In [23], total 24 traces are included in the data set and every trace records the Apps usage activity of an iPhone user for about 200 days. Each trace includes the system time stamp, the App package ID and other useful information.

I examined all the traces and found that there are total 1850+ Apps are recorded in the usage traces. However, the majority of smartphone usage time (i.e., 90%) is contributed by only 84 Apps, as depicted in Figure 2. Based on the application purpose, these popular Apps can be classified into 12 categories, as summarized in column "Rep. Apps (iOS)" in Table 2. Except for *Games*, the application usage in most of the categories is only concentrated in a few Apps.

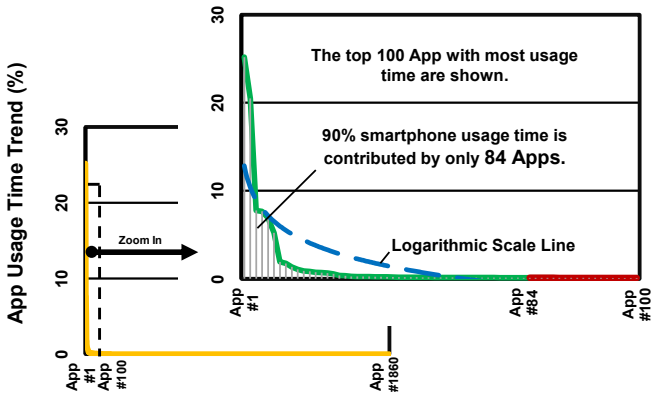

Figure 2: Usage statistics of Apps in LiveLab traces.

Table 2: Popular Apps Categories and Representatives

Category	*No.*	*Rep. Apps (iOS)*	*Rep. Apps (Android)*
System Launcher	1	SpringBoard	Android Launcher
Browser	6	Safari	Samsung Internet, Chrome
Camera	2	Photo, Video Camera	Photo, Video Camera
Email	2	Mail	Gmail
Game	41	AndryBirds, Fruit Ninjia	Angry Birds, Fruit Ninja
Navigation	3	Maps	Google Map
Messenger	3	Messenger, Facetime	WhatsApp, WeChat
Music	5	Pandora, TuneIn	Pandora, TuneIn
Phone	1	Phone Launcher	Phone Launcher
Social Nets	7	Facebook, Twitter	Facebook, Twitter
Utilities	15	Clock, Calculator	Clock, Calculator
Video	4	Youtube, CNN	Youtube, CNN

Note that the platform chosen in our research is Android, since all the Samsung Galaxy smartphone are equipped with Android. Meanwhile the traces collected in LiveLab are from iOS devices. Hence, I substitute some Apps on iOS with the corresponding versions on Android to rebuild Android user application traces, as summarized in the column "Rep. Apps (Android)" in Table 2. For example, iOS SpringBoard and iOS Safari were replaced by Android Launcher and Samsung's native internet browser, respectively. In fact, the number of Apps that need to be replaced is very small, say, only 16 among all 84 popular Apps.

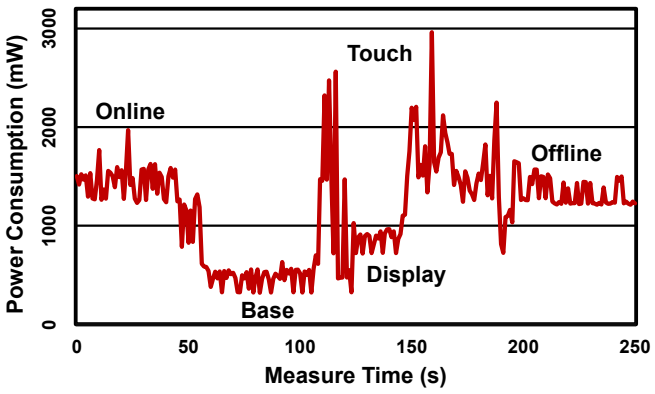

Figure 3: Galaxy S4 Wi-Fi video player power trace.

2.2.3 Smartphone Power Measurement Flow

I selected about 20 representative Apps that involve various functional components from the collected user traces in Table 2. For each App, the operations of the smartphone are divided into several working modes which cover all concerned functional components and carry necessary differences so as to derive the power consumption of each component.

Figure 3 depicts the real-time power consumption of a Galaxy S4 when running *YouTube* for 250 seconds. The operation can be divided into five working modes in our function-based measurement approach:

(1) "Online" mode, e.g., streaming a full screen video in a Wi-Fi network. All major components, including Wi-Fi, display, touchscreen and computation (CPU/GPU), are involved;

(2) "Offline" mode, e.g., playing the video locally without network supports;

(3) "Display" mode, e.g., playing static video frame without video decoding computation;

(4) "Touch" mode, e.g., finger operating on the touchscreen. The finger motion often awakes the CPU from low-power model and introduces a high peak power consumption;

(5) "Base" mode, e.g., the display being turned off and only computation and network components being active.

The power consumption of the smartphone at different working mode can be used to calculate the contribution from the major functional components. For example, the difference between the

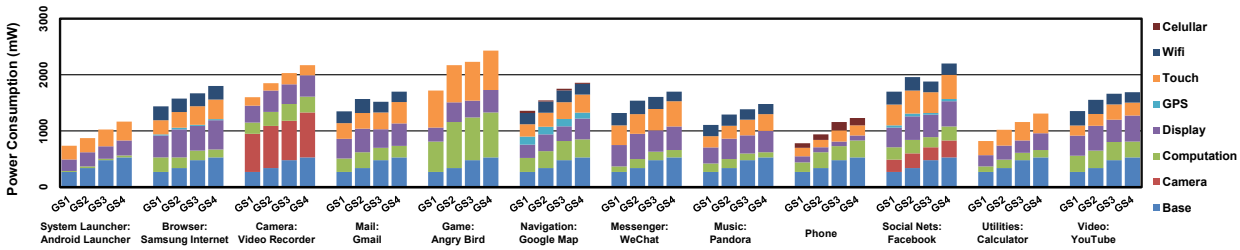

Figure 4: Representative Apps' power consumption breakdown.

power of (4) and (5) is the extra power consumed by the occasional touchscreen operation; the contribution of display component is the differences between the power of (3) and (5); the background computation power can be obtained by subtracting the power of (2) from the sum of (3), (4) and (5); finally, the difference between the power of (1) and (2) denotes the power consumption of the Wi-Fi component. Note that for different applications, the partition of the working mode must be slightly changed to cover all involved components.

2.3 SEER ANALYSIS ON EVOLUTIONARY SMARTPHONE COMPONENTS

Based on the methodology presented in Section 2.2, I measured a set of representative Apps' power consumption on all four generations of Galaxy S smartphones. Each measurement covers the App's different working modes, involving several major smartphone components. By differentiating working modes as described in Section 2.2, I can further breakdown each App's power consumption and characterize the major components' power performance through smartphone generations.

2.3.1 Smartphone Power Performance with Different Apps

In Figure 4, I listed a set of Apps power measurements under Wi-Fi network. They are measured from 12 Apps representing each popular App category. And different smartphone generation's

performance are set aside for comparison. Despite of "Base" work mode, which stay constant with smartphone generation, I divide the major component into 8 categories (3G/4G is not listed in Figure 4), such as "computation", "display", so on and so forth. Please note that, the concept of "major component" is functionality perspective. Each major component might involve with multiple smartphone hardware units. For example, when I talk about "display", the related power consumption could be introduced by both OLED screen and correlated graphic computation; when I talk about "computation", the related power consumption could be caused by CPU, also with correlated GPU computation and other processing units. Compared to traditional works focusing on peak or global average power consumption, this functionality perspective approach can well show each component's dynamic power consumption in different App scenarios.

Hence, in Figure 4, I can easily tell that, there is obvious power different from App to App. The biggest power consumption happens in Angry Bird, which reaches 1720mW∼2430mW for GS1∼GS4, and Android Launcher has only 736mW∼1160mW. This difference is defined by each App's various functionality composition and distinctive performance requirement for involved component. For example, "camera" only show with photo&video and social Apps. Also, since it's only occasional function in Facebook, it consumes much less energy than in Video Recorder and therefore smaller power consumption ratio.

2.3.2 Smartphone Power Performance with Different Generations

To have a better view for each component's power character, I sorted their average power consumption in Figure 5. Please note that, due to limited test resource, I only tested 4G network with GS4 and 3G network with GS1∼GS3. From Figure 5 I can see that, "3G/4G" network still remain the biggest power consumer. From GS1 to GS3, although I can see a possible reduction trend, the latest generation of 4G network prompts the power consumption to a new level. Also, I can see the significant power consumption of "camera" relation function, while few researches have emphasized. Moreover, since Android system bursts up the system performance for smooth touch experience, "touch" operation also introduces considerable power consumption. And due to mature technology, some components like "Wi-Fi", "cellular" (basically GSM network for voice call) and "GPS", which are considered considerable power consumer, have very ideal power efficiency.

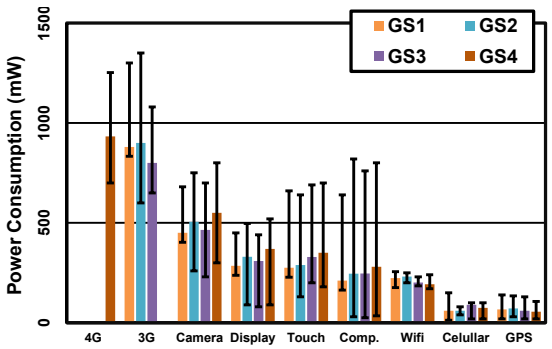

Figure 5: Major components' power consumption in smartphone generations.

Meanwhile, in Figure 5, I can also see each component' significant power variance across Apps as shown in error bar, which could be as big as ∼500mW. Hence I can tell that, in practical user's usage trace, Apps preference and usage distribution might significantly affect components and smartphones' power performance.

From the evolutionary analysis, I can see that, through smartphone evolution, different components have either improving or descending power efficiency, and within various App scenario, these component will perform distinctive power consumption.

2.4 SEER ANALYSIS ON ETHOLOGICAL SMARTPHONE USAGE

2.4.1 Smartphone User Behavior Statistic

Practical users' smartphone usage traces are the foundation for ethological analysis. From [23], besides of the most popular Apps statistic, I also extract every user's smartphone usage trace to record how each App is utilized. Since modern smartphone's battery cycle is usually one day. So I will also explore each user's usage trace in daily scope.

Actually, the smartphone users' daily smartphone interaction is more active than I imagined. For each participants, about 10∼200 different applications are accessed. And the popular applications may be active about 20∼200 times per day and the each operation time on the smartphone

Table 3: Application Daily Usage Statistics

User	A00	A07	B04	A12	A03	A08	B01	B07	B03	B00
Total App No.	90	138	39	62	226	9	18	21	10	5
App with 90% Usage No.	6	10	6	8	8	6	10	10	6	6
Average Daily Usage Time (Hour)	4.32	3.65	3.12	2.88	2.64	2.16	1.92	1.44	1.22	0.24
1st Preferred App Usage Time (Hour)	Msg. 0.60	Social 0.39	Msg. 0.68	Msg. 0.26	Video 0.74	Msg. 0.73	Social 0.34	Msg. 0.16	Msg. 0.25	Phone 0.05
2st Preferred App Usage Time (Hour)	Social 0.37	Video 0.29	Browser 0.25	Social 0.20	Msg. 0.16	Mail 0.15	Music 0.17	Utilities 0.13	Phone 0.21	Msg. 0.02

about 15 minutes to more than 4 hours. This not only confirms that significant application preference exist in user behaviors and also indicate that the overall smartphone power consumption maybe highly defined by few specific applications. For example, more than 76% of the participant have social network applications on their smartphones and averagely spend more than 100 minutes per week using those applications. And about 70% users will play videos and games at least 1 hour in total every week.

From the more than 20 users, I picked up 10 users' data as shown in Table 3. The daily usage time percentage vary from 1%∼18% among all the users. Averagely, the smartphone users might spend more than 2 hour on their smartphones and active more than 100 applications (including system services) every day. Although all the participants in this data set is college students, the usage might be more active, it really indicate that smartphone usage has become a very major activity in our daily life.

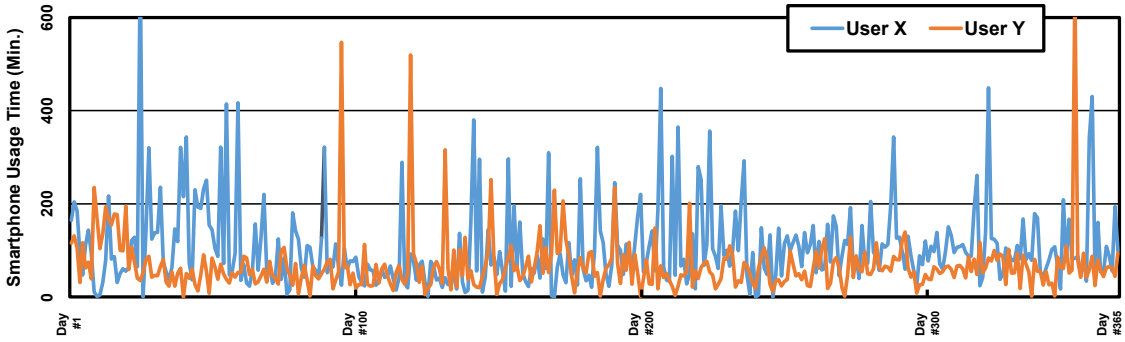

Figure 6: Two representative users' smartphone usage trace over 1 year.

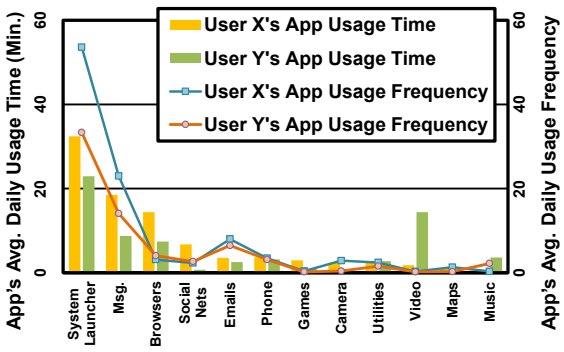

Figure 7: Two representative users' App preference.

However, during the daily usage, only 6∼11 applications are preferred, which means, these applications will account for more than 90% of all the smartphone application operation time. Despite of the smartphone system UI, most users' application are focused in communication. In Table 3, I list two of each user's of most preferred application. I can see that, in the participant user group, Messenger applications is the most preferred application, which can occupy all the applications' total activation time as much as 34%. Similarly, the Social Network applications are also high preferred.

2.4.2 Smartphone User Behavior's Impact on Energy Consumption

Given an example to show specific user's smartphone usage difference,in Figure 6, I printed two representative users' yearly usage trace, as User X and User Y, which are originally B04 and A00 profiles in Figure 6.

Figure 7 shows their average average Apps usage time and frequency. For daily App usage frequency, User X is ∼198 and User Y is only ∼130. Although both of them have periodical heavy smartphone usage over 400mins as shown in Figure 6, their average daily smartphone usage time is 77.7 mins and 69.5 mins respectively. Similarly, system launcher has the biggest usage time and frequency. And most of their Apps operation session are varying between 1 mins∼8 mins. However, these two users also have different Apps usage pattern. After 1 year, User Y has 90 different Apps records, while User X only has 39 Apps. Despite of system launcher (over

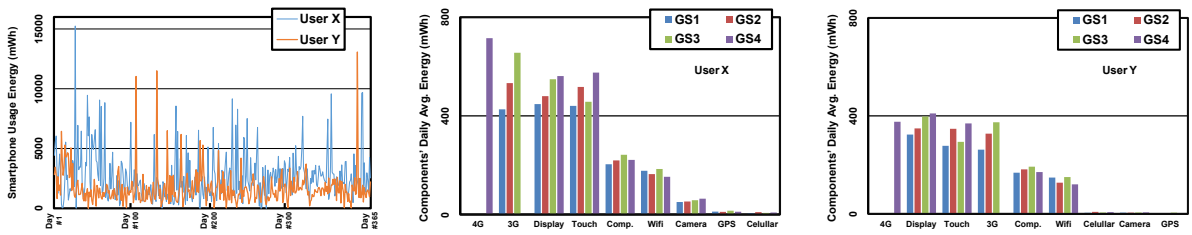

(a) Energy trace (b) User X's energy distribution (c) User Y's energy distribution

Figure 8: Energy analysis for two representative users' smartphone usage trace.

30%), User X spends most time (36%) with "messenger" and "browser", while User Y (A00) is more "video" preferred (27%), whose operation session could be as long as 40mins.

To apply these ethological characters to power analysis, I combine the usage trace with GS4's Apps power value from Figure 4. As shown in Figure 8(a), although their daily usage time difference is no more than 10mins, User X has much bigger power consumption, averaging 2611 mW, while User Y's is only 1663 mW. Given generations of smartphones from GS1 to GS4, the average daily energy consumption is 1763 mWh∼2611 mWh for User X and 1192 mWh∼1663 mWh for User Y. Although the power consumption for generations is increasing, considering the upgrading battery capacity from 1500 mAh∼2600 mAh, the daily battery usage ratio is decreased from 37%∼25% to 26%∼19%. However, in occasional peak usage scenario, the energy consumption can be as big as 15240 mW, which means, the battery needs to be recharged at least once.

To further analysis the usage trace, I further breakdown each component's daily average energy consumption with four generations' power characters. In Figure 8(b) and Figure 8(c), I rank components from descending left to right . Comparing User X and Y's component energy profile, despite of the value difference, I can also find that both profile' components have specific energy consumption weight distribution. User X is "messenger" and "browser" preferred, which have much power consumption in "touch", "3G/4G" and less in "computation". Hence in Figure 8(b) the energy difference between components is as high as 700 mWh. Meanwhile, in Figure 8(c), since "video" is frequently used, "display" and "touch" override "3G/4G" and become the biggest energy consumer; "camera"'s energy consumption is almost ignorable.

From this analysis, I can see that, smartphone user's ethology behavior will have significant impact on overall smartphone energy consumption and change each component's power consumption weight. With the evolutionary and ethological perspective, in next section, I will discuss a new approach to guide smartphone power optimization.

2.5 SEER ANALYSIS ON REALISTIC SMARTPHONE DAILY ENERGY CONSUMPTION

Based on the evolutionary and ethological analysis of smartphone power consumption, I can retrieve each component's power model correlated with App scenarios and specific user trace. Then it is possible to fit the realistic smartphone daily energy consumption. Here I show two case studies on how I can applied SEER in different energy analysis cases.

2.5.1 Case Study: A Video Player Application Preferred User

A specific usage trace is from a user (A03) preferring online video player as shown in Figure 9. Figure 9(a) shows the user's consecutive 4 weeks daily time usage with major applications. The trace example covers the smartphone usage of the user for four weeks where WiDj denotes the ith day of the jth week.The overall smartphone usage time is 0.47∼3.34 hours, averaging 2.33

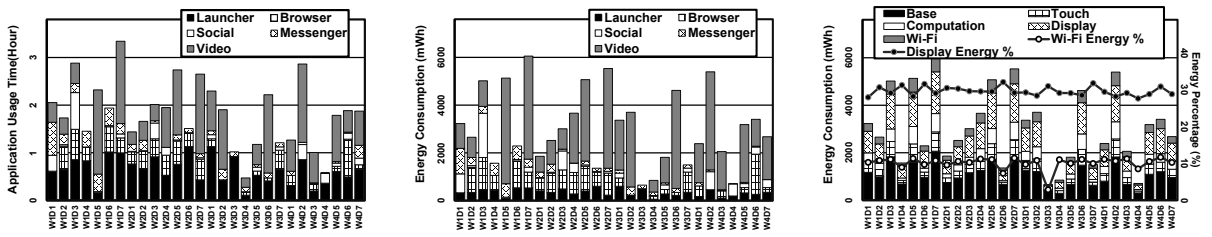

(a) Major applications' daily usage time.

(b) Major applications' energy analysis.

(c) Major function modules' energy analysis.

Figure 9: A video player preferred user's daily energy analysis.

hours per day. The usage time of video is about 0.19∼1.76. Although there 6 days without video application activation, the averaging usage is still as high as 0.72 hours per day. The messenger application usage ration is about 33% of the total daily usage time.

Considering the energy consumption as shown in Figure 9(b). The average energy consumption is about 1914mWh, and the daily battery usage is 6%∼58%, averaging 29%. Since the Wi-Fi power consumption does not vary significantly among applications, with this user's more energy consuming application preference, the average Wi-Fi module's energy consuming ratio is only about 10.9% as shown in Figure 9(b) 9(c).

With low network energy consumption, display reaches a very high energy ratio of 27%∼32%, which becomes a bottle neck in this condition. Please note that, in Figure 5, rather than display components, there are some modules like "camera" and "touch" have higher peak power consumption and variation range. However, their practical energy consumption also depends on their utilization ratio. And among all the smartphone components, "display" always has the biggest utilization ration. From different cases, I found that, the biggest power consumer is "display", which spends 30.1% of the total smartphone energy.

2.6 CHAPTER 2 SUMMARY

From the evolutionary analysis, I can see that, through smartphone evolution, different components have either improving or descending power efficiency, and within various App scenario, these component will perform distinctive power consumption. From this analysis, I can see that, smartphone user's ethology behavior will have significant impact on overall smartphone energy consumption and change each component's power consumption weight. And in our preliminary results analysis in Section 2.5, I shown that with the evolutionary and ethological study, I can reveal the realistic energy consumption condition.

I found that over the four generations of Samsung Galaxy S series smartphones, the average power consumption of the whole smartphone increases by 38.2% when the device is connected to a Wi-Fi network. The power efficiencies of Wi-Fi component and GPS component, however, improve by 21.8% and 25.8%, respectively, contributing to less than 15% of the total smartphone

power. Although the power efficiency of 3G component is enhanced on Galaxy S3 w.r.t. Galaxy S2, such an improving trend is broken by the introduction of 4G component. The biggest power consumer is “display”, which spends 30.1% of the total smartphone energy. Nonetheless, for most components like CPU, GPU, and GPS, I observed a continuous improving trend of the component power efficiency, implying a better energy-saving design in the next-generation Samsung Galaxy S series smartphone.

3.0 OLED DISPLAY POWER OPTIMIZATION IN HARDWARE LEVEL

In previous Chapter 2, "SEER"shows that averagely, "display" is the biggest power consumer is , which spends 30.1% of the total smartphone energy. From this Chapter, I am going to propose a set of power optimization techniques targeting OLED display, which is considered the most popular and promising display technology in modern smartphone design.

In this section, Section 3.1 first gives OLED technology's preliminary and related research works. Section 3.2 presents the proposed hardware level OLED power optimization technique – DVS friendly OLED driver design and its correlated Fine-grained DVS scheme (DiViSi). Section 3.3 summaries this chapter.

3.1 OLED PRELIMINARY AND RELATED WORKS

3.1.1 OLED Preliminary

3.1.1.1 OLED Color Displaying Mechanism and Drivers A chromatic color tunable OLED pixel is composed of three basic cells corresponding to RGB color space, i.e., red, green and blue. Figure 10 (a) shows a popular OLED pixel structure where the three basic cells are built on the same substrate and aligned side-by-side. Each cell is driven by an independent driver, though all drivers share the same power supply. Since the emitting efficiency of the cells varies with different colors, the sizes of the cells are skewed to ensure the balanced color composition [1]. The equivalent schematic of an OLED cell is shown in Figure 10 (b), including a capacitor, an ESR (electrical series resistor), and a light emitting diode. The internal capacitance C_{cell} comes from the organic films, whose thickness is about 100 200nm. It corresponds to a typical unit capacitance of

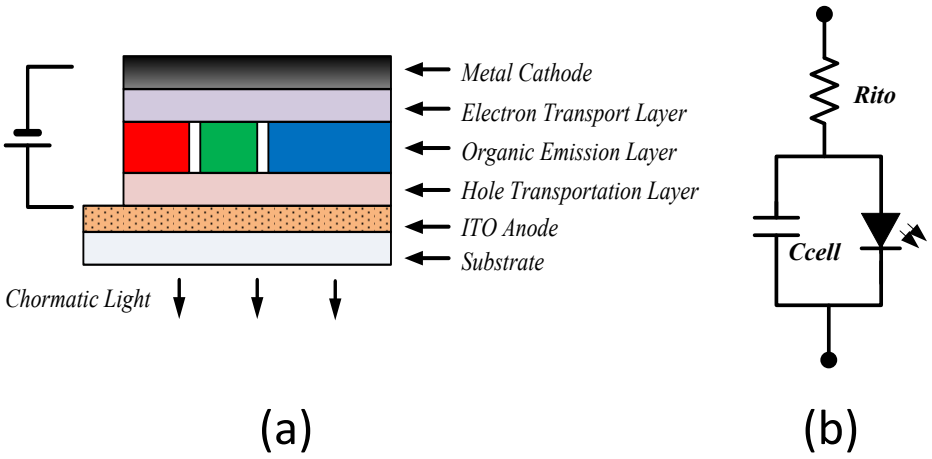

Figure 10: OLED Structure. (a) Equivalent schematic of an OLED cell. (b) Structure of a RGB color tunable OLED.

200∼400pF/mm^2. The ESR is mainly from the electrodes, which is made of transparent indium-tin-oxide (ITO). A typical square resistance of ITO layer R_{ITO} is about 15Ω/sq. The current-voltage ($I-V$) characteristic of an OLED cell is determined by dopant types and cell sizes [25].

The light emitting efficiency of an OLED cell (η) is measured by the ratio between the cell luminance L and the power consumption $P = I{\cdot}V$. Here I and V are the current and the voltage through the OLED cell, respectively. The luminance of an OLED cell is proportional to the magnitude of driving current while the displaying efficiency varies for different colors: to achieve the same luminance, the ratio of the required power consumptions of red, green and blue OLED cells is about 1:1:2 [19]. The display of OLED pixels is usually controlled by two different methods, namely, pulse-width-modulation (PWM) and amplitude-modulation (AM). AM is more popular than PWM in OLED display panel designs because the operations of electronic switches in PWM could incur a huge current spike on inner OLED capacitance. It may damage the OLED cells and adversely affects their life time.

From a circuit perspective, OLED driver circuits can also be divided into two types, namely, PMOLED (passive matrix) and AMOLED (active matrix). As shown in Figure 11(a), each OLED

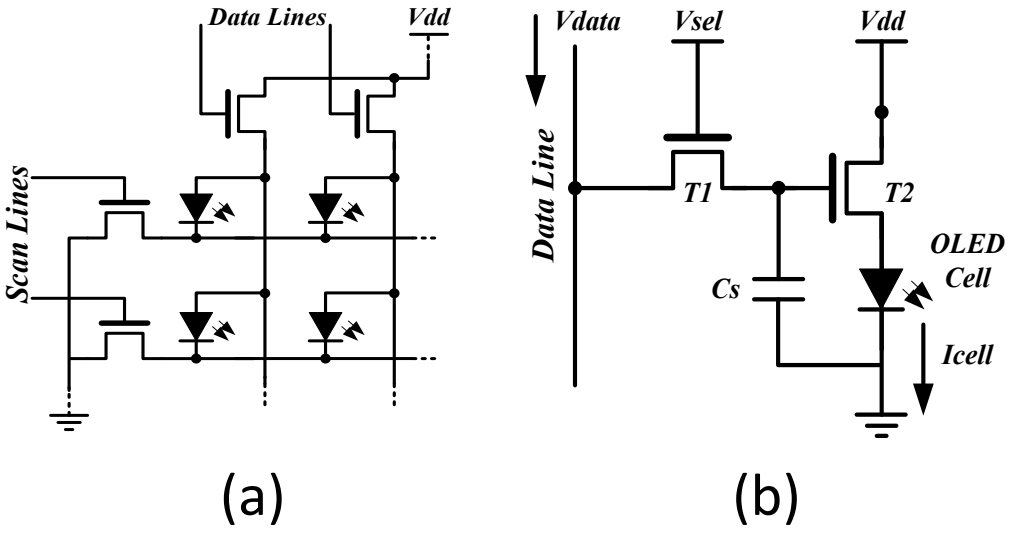

Figure 11: OLED driver structures: (a) PMOLED panel. (b) Basic AMOLED driver [1].

pixel in PMOLED is selected by turning on the selection transistors of the corresponding row and column [1]. However, the voltage drop along the column metal wires can be significant so that a high Vdd must be applied to compensate the brightness of the pixels at the far ends of the array. Such a design, however, lowers the power efficiency of PMPLED and shortens the OLED cell lifetime. Also, the non-uniform supply voltages on each pixels causes the severe color distortion issue when OLED panel size is large, i.e., $<$ 3-inch. A conventional AMOLED driver design is shown in Figure 11(b). The OLED cell driving current I_{cell} is supplied by a driving transistor T_2 whose gate voltage is programmed by V_{data} through a select transistor T_1. The display status of the OLED cell can be maintained by a storage capacitor C_s even after T_1 is unselected. Compared to PMOLED designs, AMOLED has lower power consumption and no restrictions on either the OLED panel size or resolution. The variations of V_{data}, however, may result in the nonlinear change of I_{cell}. In other words, color distortions occur immediately right after the V_{data} is scaled.

3.1.1.2 Statistic OLED Power Consumption Modeling

During displaying, the TFT drivers are programed to supply the required driving current through each OLED cell. By adjusting the magnitude of driving current, fluorescent light emitted from the OLED cells are tuned into specific strength. A simple model of the power consumption of an OLED cell is [1]:

$$P_cell \approx I_{cell}(C) \cdot V_{dd} \tag{3.1}$$

Here I_{cell} is the current through the OLED cell. The magnitude of I_{cell} is determined by the RGB color strength C, i.e., a value between 0 and 255 in RGB color space. V_{dd} is the supply voltage. The power consumption of the whole OLED screen is the sum of the contributions from all display pixels, or [19]:

$$P_{display} = \sum_{i,j=0}^{p,q} \left[P_{cell}^{i,j}(R) + P_{cell}^{i,j}(G) + P_{cell}^{i,j}(B) \right] \tag{3.2}$$

Here $P_{cell}(R)$, $P_{cell}(G)$ and $P_{cell}(B)$ are the power consumptions of the red, green, and blue OLED cells in an OLED pixel, respectively. p and q are the row and column numbers of the pixels on the OLED screen, respectively. Note that the luminance of an OLED cell is proportional to the I_{cell} and affected by the color-dependent lighting efficiency [19].

3.1.1.3 HVS-Aware Video Quality Assessment

Different video quality assessment (QVA) methods have been investigated in the researches on human visual system (HVS) [14]. For instance, structural similarity index (SSIM) was proposed to quantitatively measure the image distortions by comparing the similarity between two images: For a color image, an image matrix is created as MSSIM = [R:G:B], where R, G, B are the matrices of the luminance of the red, green and blue cells of every pixel on the OLED panel. The SSIM of the new image X at the scaled V_{dd} w.r.t. the original image Y at the normal V_{dd} is calculated as [26, 27]:

$$SSIM = \frac{(2\mu_x\mu_y + C_1)(2\sigma_{xy} + C_2)}{(\mu_x^2 + \mu_y^2 + C_1)(\sigma_x^2 + \sigma_y^2 + C_2)} \tag{3.3}$$

Here μ_x and μ_y are the average of the image matrices of the new image X and the original image Y, respectively; σ_x and σ_x are the variances of each image matrices, respectively; σ_{xy} is covariance. C_1 and C_2 equal 2.55 and 7.56 for RGB color space, respectively. SSIM value denotes

the image quality: 1∼0.98, 0.98∼0.96, and 0.96∼0.94 means high quality, medium quality, and low quality, respectively. Below 0.94 means unacceptable. In our later proposed OLED power optimization technology, SSIM is widely used for visual quality evaluation and control.

3.1.2 Related Works

As proved in Chapter 2, although the power efficiency of OLED has been significantly improved since it was invented, OLED screen is still one of the major contributors to the overall power consumption of smartphones. Many OLED power optimization approaches have been proposed.

First of all, there are also lots of power management methods inherited from LCD technology requiring minimum analysis works. Automatically shutting down the display when the electronic is not being used is the most classic display power reduction method [28, 29]. Similarly, global luminance dimming has been widely used in modern mobile device power management designs, i.e. in [15], Cheng utilized the contrast scaling, [30] designed dedicated dimming policies. In [1], HP Lab proposed to dim the non-focal area in the image for OLED power saving. However, identifying the focal area becomes very challenging in a complex image. And global voltage scaling was also introduced to adaptively adjust the OLED supply voltage based on the display content [12]. However, these methods significantly degrade the display visual quality [27].

As aforementioned, OLED pixel power consumption is directly determined by the displayed color [19]. Therefore, more OLED power research work were trying to leverage the display content and the power consumption on OLED display panel. Hence, color remapping becomes a very efficient approach in OLED power management. Dynamic tone mapping (DTM) was first introduced in image processing and computer graphics to map one input color set to another through mapping functions such as linear scaling and gamma correction. In classical image processing applications like high dynamic range image and video processing, DTM is used to tune the pixel explosion and color effect for display quality improvement. Since the power consumption of an OLED screen is color dependent, the concept of DTM has also been introduced to OLED power management [18, 31]. And some optimization schemes were proposed for UI design and web browsing [13, 17]. However, all these researches mainly focus on the OLED power consumption of static image displaying. And the user's visual experience is not well considered.

Human visual system quality assessment, HVS, theory was introduced to real-time multimedia device design to measure display quality by taking into account the human factors [14]. For example, both SSIM [26, 27] and MSE (mean squared error) [12] are used to direct the static image quality in LCD power managements. Although the computation cost of SSIM is about 2 of MSE's, SSIM has shown some advantages over MSE, including precise image evaluation for human perception and clear evaluation standard. Hence, the visual quality assessment with HVS, (especially with SSIM), and OLED power character utilization, become two major tasks in recent display power optimization research.

3.2 DIVISI: QUALITY-RETAINING OLED FINE-GRAINED DYNAMIC VOLTAGE SCALING

Based on the understanding of OLED structure and mechanism, I started the OLED optimization from the hardware level, which improves the driver circuit performance with effective user visual perception quality retaining. In this section I propose a new *dynamic voltage scaling* (DVS) technique with an optimized cell driver design to save the OLED power consumption with controllable HVP-quality degradation.

3.2.1 OLED Driver Circuit Improvement

3.2.1.1 DVS-Friendly OLED Driver Design DVS technique has been widely used in low power design. In conventional OLED driver design in Figure 12(b), the scaling of V_{dd} inevitably degrades the driving ability of transistor T_2 and causes color distortion of the OLED cell. In this section, I propose "DVS-friendly" driver design, which can reduce I_{cell} degradation or even maintain the original magnitude of I_{cell} at the scaled V_{dd}.

Figure 12 illustrates the conceptual schematic of our proposed DVS-friendly driver design. Unlike the conventional driver using V_{data} as the programming signal, here the OLED cell luminance is programmed by a current I_{data}. During programming stage, V_{sel} is raised to high. V_{ctrl} is pulled down to turn off T_3 and ensure no current flowing from V_{dd} to the OLED cell. I_{data} passes

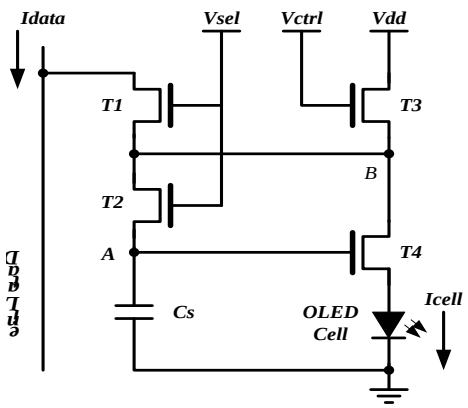

Figure 12: DVS-friendly AMOLED driver design

through T_1 and the bias conditions of transistor T_4 is setup to supply the desired current through the OLED cell, e.g., $I_{cell} \approx I_{data}$. The gate voltage of T_4 is recorded on capacitor C_s. During displaying stage, V_{sel} is pulled down to LOW and I_{data} is cut off from the driver. V_{ctrl} is raised to turn on T_3. The OLED cell continues working in emission period. Because the bias condition of T_4 is recorded by C_s, I_{cell} keeps the same as the one in programming stage.

Figure 13 depicts our simulation results of the relationship between I_{cell}'s and the programmed gray levels for both conventional OLED driver design in Figure 13 (b) and my DVS-friendly design. Gray level (horizontal axis) denotes the normalized programming signal strength (V_{data} or I_{data}) over the maximum level. (Actually, the gray level is a concept from the monochromatic image to indicate the black color luminance levels. Later people use this to indicate the image signal about luminance. In RGB color space, the absolute maximum gray level is 255.) Vertical axis is I_{cell} whose maximum magnitude is 10 μA in DVS-friendly design. Figure 13 (a) shows that in conventional OLED driver design, when Vdd reduces from the normal level = 15V, I_{cell} decreases substantially and directly causes color distortions. As shown in Figure 13 (b), in DVS-friendly design, I_{cell} shifts from the required magnitude only when the gray level is high. Even at the high gray levels, the degradation of I_{cell} is still much less than that of conventional OLED design.

Compared with the conventional AMOLED driver design, the OLEDs are directly programed by the current mirror, which makes the OLEDs' programming more precise and the capacitance

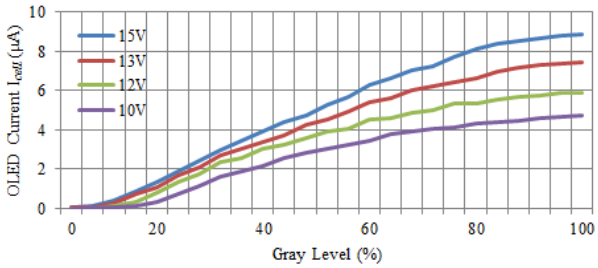

(a) *Conventional AMOLED Driver*

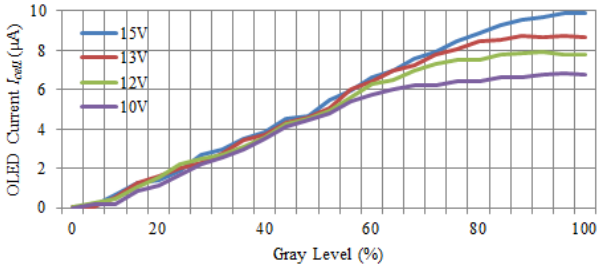

(a) *DVS-Friendly AMOLED Driver*

Figure 13: Relationships between the I_{cell} and gray level of DVS-friendly OLED driver design at different V_{dd}s.

charging more stable. When the supply voltage is scaled, the programing value maintains at the same value in some range. Moreover, when some image processing mechanism are applied to the image data in display RAMs, the processed output can directly applied in to the OLED currents I_{cell}. In dynamic voltage scaling behavior, this driver can react faster and more precise than the conventional AMOLED drivers.

Figure 14 compares the images shown on the OLED panels with conventional and DVS-friendly drivers, respectively, at a scaled V_{dd}= 11.2V. Due to the global color distortions and luminance loss, significant image quality degradation is observed in Figure 14 (a) (conventional de-

(a) Conventional

(b) DVS-Friendly

Figure 14: Image quality comparison for different OLED driver designs. V_{dd}=11.2V.

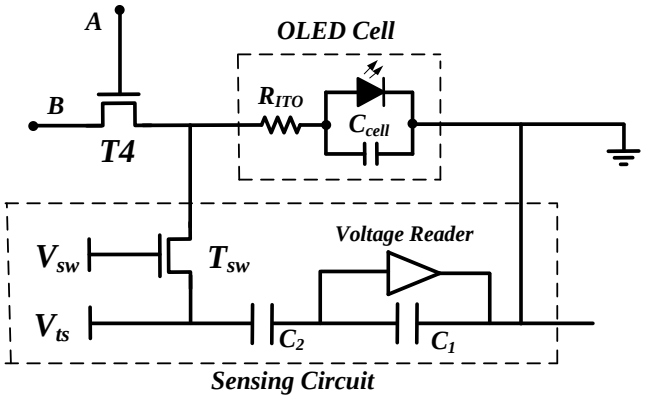

Figure 15: Non-uniformity sensing circuit.

sign). The SSIM of Figure 14 (a) is only 0.8209, categorized as "unacceptable". In fact, to achieve a SSIM = 0.98 in conventional design, the V_{dd} must raise to 14V. As a comparison, the image in Figure 14 (b) (DVS-friendly design) has an SSIM = 0.9863, categorized as "high quality".

3.2.1.2 Peripheral Circuit Design for Reliability Enhancement on Non-uniformity and Aging

In OLED driver design, two biggest challenges are the manufacturing non-uniformity and aging effect. Hence, I propose a sensing circuit to detect the non-uniformity of display panel incurred by the device variations and/or aging of OLED cells and TFTs, as shown in Figure 15. During the detection of OLED cell aging, T_4 and T_{sw} are turned off to separate the cell from the sensing circuit. Then V_{ts} is applied to charge the voltage across C_1 to V_1, which can be obtained by the voltage reader. After that, V_{ts} is turned off and T_{sw} is turned on to allow the charge sharing among C_{cell}, C_2 and C_1. At this time, the voltage across C_1 changes to V_2. The degraded C_{cell} can be calculated by:

$$C'_{cell} = \frac{(V_1 - V_2) \cdot C_1 \cdot C_2}{V_2 \cdot C_2(V_1 V_2) \cdot C_1} \tag{3.4}$$

Eq. (3.4) can be used to derive the degradation of the OLED cell emitting efficiency.

During the detection of TFT process variations, the OLED cell will be programed by I_{data} to a certain level first. Then Tsw is turned on to connect the sensing circuit to the OLED cell while

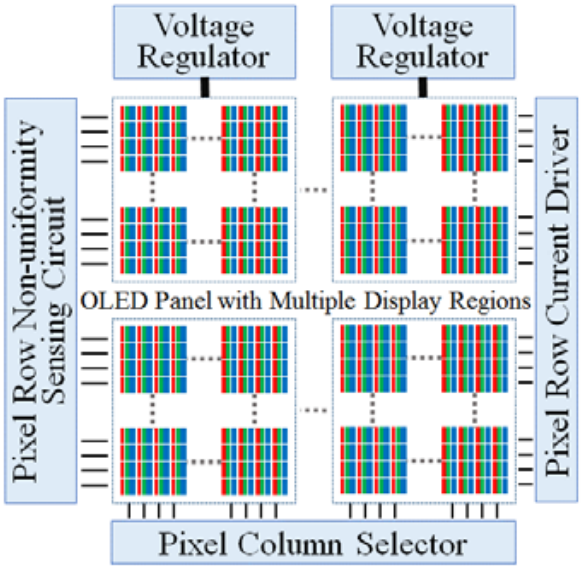

Figure 16: Display panel architecture.

T_4 is shut off. I use V_3 to denote the voltage across C_1 once the charge sharing process completes. The I'_{data} through the OLED cell during the programming stage can be derived as:

$$I'_{cell} = \frac{2 \cdot V_3 \cdot (C_1 + C_2)}{C_{cell} \cdot R_{ITO}} \tag{3.5}$$

The degraded real-time OLED cell luminance L' is proportional to C'_{data} and I'_{data}. Thus, by using our proposed sensing circuit to scan all OLED cells, I can construct the non-uniformity map of the display panel and build a new mapping relationship between the programming current I_{data} and the target luminance of the OLED cell L'. This mapping relationship will be leveraged to compensate the aging effect and the device variations of OLED panel.

Figure 16 shows a possible display panel architecture which is divided into multiple display regions with their own reliability sensing circuit and power supply. Such a design can reduce the response variation of OLED cell under the DVS scheme by leveraging the locality of manufacturing variability. Also, as I shall show in Section 3.2.3.1, the partitioned voltage supply design enables *local DVS scheme* that offers a higher power saving efficiency w.r.t. *global DVS scheme*.

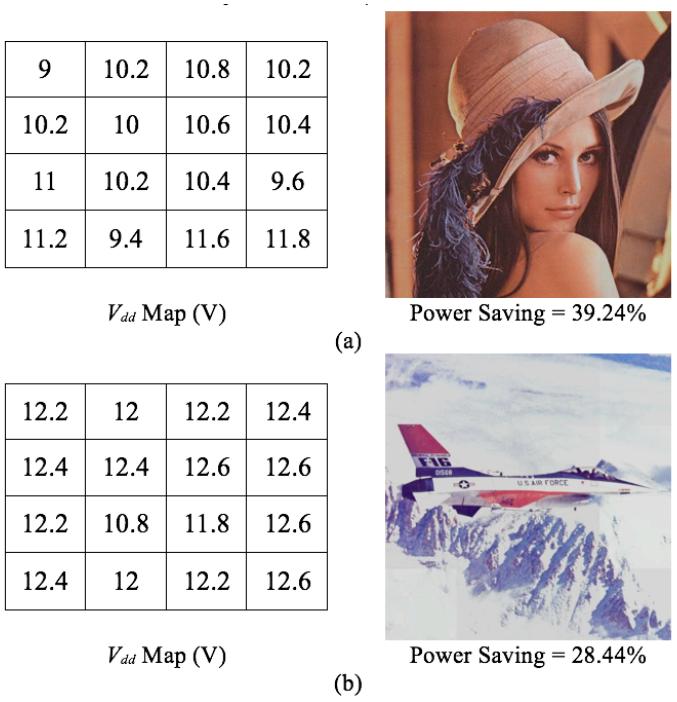

Figure 17: Effectiveness of different techniques. (a) Lena. (b) F16.

3.2.2 Fine-grained Dynamic Voltage Scaling

In the global DVS scheme, increasing V_{dd} reduces the number of pixels that cannot be fully compensated by paying the degradation of power efficiency. FDVS, however, allows V_{dd} adjustment at a smaller granularity and improves the power consumption of OLED panel and image quality. Fig. 12 shows images of Lena and F16 at SSIM = 0.98 after FDVS is applied. The DVS-friendly driver design is adopted. Images are divided into 16 display areas whose Vdds are adjusted separately and no color remapping is applied. The Vdd maps of every display areas are also shown besides the images. As shown in Figure 17, the OLED power saving of Lena is raised by 43.1% (from 27.41% to 39.24%), compared to the global DVS scheme with DVS-friendly driver designs. In F16, the power saving is raised by 25.9% (from 22.57% to 28.44%). The lower absolute power saving is because the major color occupies most of area in F16. Small Vdd adjustment spaces are left to each display areas, as shown in the map of Fig. 12(b). Human visual perception, however, is mainly affected by the major colors brightness.

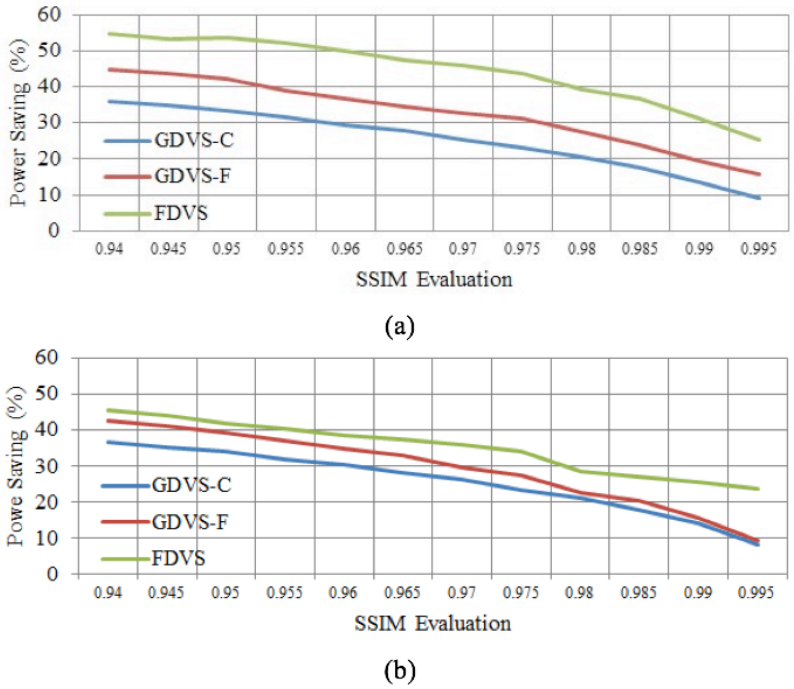

Figure 18: Performance evaluation of different techniques. (a) Lena. (b) F16.

Figure 18 summarized the power saving and the image quality of different technique combinations, including conventional OLED driver design with global DVS (GDVS-C), DVS-friendly driver design with global DVS (GDVS-F), and DVS-friendly driver design with fine-grained DVS (FDVS). Here I did not evaluate the effects of color remapping because it heavily relies on the specific software and hardware designs and does not directly accounts for the total OLED power consumption. Substantial power saving is obtained by our DVS-friendly OLED driver designs and FDVS technique compared to the global DVS technique with conventional driver designs.

3.2.3 Real-time Optimization for Video Streaming

After achieving the hardware level breakthroughs in Section 3.2 and Section 3.2.2, the biggest changeling in the proposed project becomes system-level realizations in the practical real-time streaming. In this section, I presented the real-time optimization for the DVS technique system-level research is partitioned into the following two aspects: 1) spatial and temporal constrains analysis; and 2) real-time OLED power management technique.

Voltage Map

5	5.2	6	5.3
7.2	7.4	6.6	5.6
10.6	9.2	7.5	8.8
13.3	13.1	10.8	9.4

(a)

Voltage Map

5.8	6.8	7.8	5.8
7.4	9.2	9	6.6
13.2	11.8	11.4	10
13.8	13.4	13.2	11.4

(b)

Figure 19: SSVO results including voltage map. (a) Without global SSIM control. (b) With global SSIM control.

3.2.3.1 Spatial and Temporal Constraints Analysis

As the first sub-task, I propose *spatial supply voltage optimization* (SSVO) and *temporal supply voltage optimization* (TSVO) to accommodate the application constraints of DVS scheme at physical and time domains, respectively

3.2.3.2 Spatial supply voltage optimization (SSVO) for intra-frame DVS

As shown in Figure 17; the OLED panel can be partitioned into multiple display regions (see Figure 16) to achieve *local DVS scheme*. Each display region has its own supply drivers that can be controlled independently (similar to LCD local dimming technique [30]. Since the human visual system is more sensitive to the major objects in discontinuous areas [32], the V_{dd} of each display region is adjusted only based on the RGB components of the parts of the major object(s) in the region. For the display regions that do not include the major object(s) or the maximum luminance is low, an aggressive V_{dd} scaling can be applied to obtain the maximum power saving with the minimum impacts on the image's structural similarity [33]. I refer to this technique as SSVO.

When V_{dd} decreases, the colors of the pixels with high luminance are distorted first. HVP index, i.e., SSIM, can be used to guide the voltage assignment on the display regions. However, I found that satisfying SSIM requirement in each region does not necessarily guarantee the SSIM satisfaction at frame level. As shown in Figure 19(a), the voltages of every region has been separately scaled for a local SSIM=0.98. However, the global SSIM of the whole image is only 0.88.

Sharp edges between two adjacent regions can be easily observed. Raising the voltage of every display region helps eliminating these edges, as shown in Fig. Figure 19(b). Hence, a second round V_{dd} adjustment is necessary to ensure the SSIM at frame level.

3.2.3.3 Temporal supply voltage optimization (TSVO) for inter-frame DVS SSVO shows that the optimal V_{dd} assignment of an OLED panel is decided by the color profile of display content, and hence, varies from frame to frame in video streaming applications. To search the optimal V_{dd} assignment in time domain, I propose TSVO technique, which can be formulated below:

The objective of TSVO is to minimize the total power of an OLED panel, or:

$$Min(\sum_{i=1}^{n} \sum_{j=1}^{m} P_{ij}) \tag{3.6}$$

Here, n is the size of frame set; m is the number of the partitioned regions in the OLED panel; and P_{ij} is the total pixel power in display region (i, j), or $P_{ij} = \sum_{s=1}^{w} \sum_{t=1}^{h} v_{ij} c_{st}$. w and h are the width and height of the OLED panel, respectively. c_{st} is the current flowing through pixel (s, t) in the region (i, j). $v_i j$ is the supply voltage applied on the region (i, j).

The constraints of TSVO mainly come from the following two perspectives:

(1). *HVP-quality*: For every frame fi, i = 1,,n, its global SSIM must be above the required SSIMreq, or:

$$SSIM_i \geq SSIM_{req} \tag{3.7}$$

(2). *Voltage regulator response limit*: The maximum voltage that can be adjusted for the voltage regulator between two video frames is usually limited. It constrains the largest voltage difference between the supply voltages of a display region in two adjacent frames.

The output of TSVO is a set of optimal voltage levels which do not violate the above two constraints and achieve the minimum total power of the OLED panel as $V = v_{ij} \mid i = 1, ..., n, j = 1, , m$.

The main challenge in SSVO is constructing the interactive optimization flow between the global and local SSIM controls. Increasing the number of display regions will exponentially raise the complexity of the V_{dd} assignment problem. Therefore, a heuristic optimization method becomes necessary.

TVSO can be solved by *integer linear programming* (ILP) solver. However, similar to SSVO, the incurred computation cost can be extremely high when the problem size is large, i.e., for a fine-grained region partitioning or a large size OLED panel [34, 35]. Thus, a heuristic optimization method is also desired. Moreover, the detailed hardware specifications may complicate the optimization constraints of TVSO. For instance, the adjusting rates of a voltage regulator when increasing and decreasing the output voltage are usually asymmetric: For TPS61060 voltage regulator [36], 2V and 0.5V maximum output changes can be achieved at rising and failing edges, respectively, between two frames at a frame rate of 30fps. When the frame rate rises to 60fps, the corresponding maximum output changes reduce to 0.8V and 0.2V, respectively, leading to a more restrict constraint on V_{dd} change.

3.2.4 DiViSi with Real-time OLED Power Management for Video Playback

The power management techniques proposed can be easily applied to offline OLED power management. For instance, power management scheme can be pre-optimized and delivered together with the video content, e.g., offering the customized DTM policies for the viewers mobile device when he/she downloads video from $YouTube$. However, for online or real-time video streaming in which the display contents are generated on-the-fly, the procedure of downloading/capturing, decoding, processing and displaying must be completed within the tight time interval between two adjacent frames. Meanwhile, satisfactory HVP-quality shall be also maintained no matter if the power management is applied or not.

I propose a real-time power management flow for OLED panels, as illustrated in Figure 20. Decoding buffer starts with the decoded frames that have not been processed by any power management schemes, i.e., frames i to i+b, which are in one process group. If no real-time power management is applied, video display will start at t_0. In our real-time power management scheme, I slightly delay the display to t_2 so that I can generate the DVS or DTM schemes for the buffered frames within this small delay dynamically: for the group of frames i to i+b, the power management processing starts at t_1 at which all frames have been decoded; the processing ends at t_1 at which frame i becomes ready for display. Similarly, the same process on frames i+b to i+2b repeats on [t_2, t_2] to ensure a smooth video displaying.

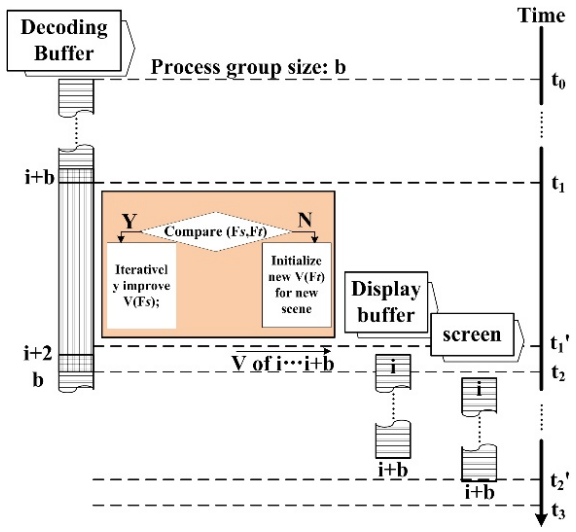

Figure 20: Real-time Flow.

During [t_1, t_1], the first and the last frame of the group of frames i to i+b are identified as Fs and Ft, respectively, and compared. If they are similar, or say, in the same scene, the DVS or DTM schemes of all the frames in the group may be optimized based on only F_s; otherwise, the location of scene transition will be detected so that different optimizations can be applied to the different scenes. Time interval [t_1, t_2] is used for video processing.

3.3 CHAPTER 3 SUMMARY

In this part of work, I proposed an optimal DVS optimization method to manage the power consumption of OLED panels in video stream applications. Two optimization steps spatial supply voltage optimization and temporal supply voltage optimization guarantee the real-time video quality while receiving the minimal energy consumption. The experimental results on four typical test benches show that comparing to conventional global DVS solution, our technique saves 19.05% 49.05% OLED power on average while maintaining a high display quality (SSIM ¿ 0.98).

4.0 OLED DISPLAY POWER OPTIMIZATION IN SOFTWARE LEVEL

In previous Chapter 3, "DiViSi"shows that averagely, an effective power optimization have be achieved by the driver circuit optimization. However, not all the OLED equipped devices can benefit from this approach, especially those marketed devices. In this Chapter, I am going to propose a pure software optimization based power optimization scheme, which has extremely power optimization overhead and optimal power saving result.

The rest of this chapter is organized as follows: Section 4.1 first the improved OLED power model regarding highly dynamic video streaming condition, which allows me to have a better foundation for the software optimization. Section 4.2 shows the proposed software level OLED power optimization technique – video category based dynamic tone mapping (DaTuM). Section 4.4 summarizes this chapter.

4.1 IMPROVED DYNAMIC MODEL FOR OLED POWER CONSUMPTION

Precise characterization of dynamic OLED power consumption is essential to the analysis and optimization of real-time power consumption of OLED display, especially for the software based optimization. In [19], an OLED power model is measured by gradually increasing the strength of static monochromatic color images red, green, and blue (RGB), respectively. Following the same method, use Monsoon power meter to measure the static power consumption of the 4.8" Super AMOLED screen of a Samsung Galaxy S3, as shown in Figure 21. Given a C (color strength value) in any RGB channel, the pixel power consumption $P_{static}^{(i,j)}(S)$ in Eq. (3.2) can be:

$$P_{Static}^{(i,j)}(S) = \alpha \times C^3 + \beta \times C^2 + \delta \times \mathbf{C} + \lambda \tag{4.1}$$

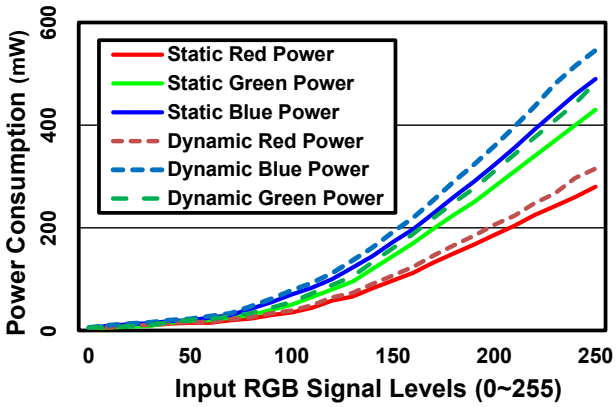

Figure 21: Comparison of OLED statistic and dynamic power models on Galaxy S3.

Here the characterized coefficients α, β, δ, λ vary in the specific RGB color channel. The approximation errors of the power model in Eq. (4.1) w.r.t. the measurement data is less than 4% when the OLED screen displaying a static frame. However, when displaying video streams, this power model shows about 10% errors compared to the measured power. Thus, rather than measuring gradual color transitions, I insert fast alternating black frames into the tested monochromatic color frames to simulate flashing display content in video streams. I set the speed of the alternating frames to 15 fps (frames per second), which is similar to normal smartphone video streaming speed. The measurement results of our dynamic power model characterization are shown as the dash lines in Figure 21. It is observed that there is significant difference between the OLED power models obtained from the static and dynamic power measurements. This discrepancy indicates the impact of the inter-frame color difference on OLED screen power consumption.

I then change the color strength of the tested frames while still maintaining the inserted alternating black frames. Our measurement shows that the dynamic power consumption of the OLED screen is almost proportional to the inter-frame color difference. Hence, I propose a modified dynamic OLED power model as:

$$P^{(i,j)}_{Static}(C_n) = R \times |C_n - C_{n-1}| + (\alpha \times C^3 + \beta \times C^2 + \delta \times \mathbf{C} + D) \tag{4.2}$$

Here C_n and $C_{(n-1)}$ are the color values of the current and the previous frames, respectively. R is a constant related to the frame rate. By leveraging the improved power model in Eq. (4.2), I can precisely calculate the dynamic power consumption of OLED screen for video streams. Based on the real measurement on $\sim$50 video streams, I found that the approximation error of our improved OLED dynamic power model is below 5.3%. In the rest of this proposal, all OLED power simulations are based on this model.

4.2 DATUM: VIDEO CLASSIFICATION BASED DYNAMIC TONE MAPPING

During the improving dynamic OLED power model and analyzing OLED display power consumption of various video streams. I found that video streams from the same video category share many common power consumption features of OLED displays. Thus, I am able to build a Hidden Markov Model (HMM) classifier to categorize videos based on power display power characteristics. Using the HMM classifier, I propose a video classification based dynamic tone mapping (DaTuM) scheme to remap output color range and minimize the power-inefficient color compositions on OLED screens for power saving. In this Section, I will discussion the details of the proposed DaTuM technique.

4.2.1 Video Classification with HMM

Based on different features of a video stream, e.g., embedded text, audio track and visual content, video classification techniques have been proposed in order to precisely describe the video content, automatize the classification to manage unknown videos, and narrow down the viewer's choice [37]. Many classification algorithms, such as GMM (Gaussian Mixture Model), Bayesian networks, rule-based classifiers, label, etc., were also developed [38]. The classification criteria for a specific video category generally describe the above features shared by the video streams under each category. However, these methods often ignore the temporal relation between the frames and scenes in a video stream, which is also a very helpful cue to understand the video content.

To solve this problem, HMM (Hidden Markov Model) was proposed to classify image, video, and audio [39, 40, 41, 42] based on their temporal patterns. In particular, HMM is able to effectively analyze the relationship between the frames and scenes in video classification. In this work, I propose an HMM classifier to analyze the temporal power features of the video streams.

4.2.2 Video Streams' OLED based Power Profile & Features

By leveraging the proposed OLED power model, I analyzed the power features of the video streams from 4 representative categories, i.e., *movie trailers*, *cartoon clips*, *video games*, and *news reports*. Figure 22 illustrates the simulation results of three typical OLED screen power consumption trace examples from each video category. The result of each video stream is represented by different color. Every video stream has 1500 frames, lasts 2∼3 minutes long with a frame rate of 10 15 fps.

4.2.2.1 Video Stream Power Profile on OLED Display Panel During our power feature extraction, instead of examining power consumption trace of a video stream over every single frame, I propose a sampling scheme of three steps, namely, scene detection, key frame selection, and power profiling. In scene detection step, scene transitions can be detected by monitoring the significant change of SSIM (structural similarity index), which is a human visual based image quality metric [27]. The frequency and magnitude of SSIM changes can be used to detect flashing scenes

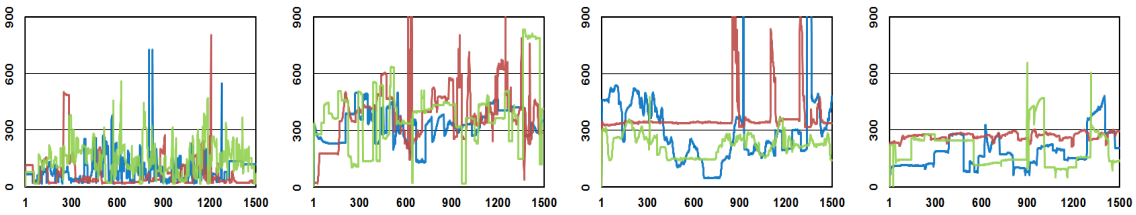

(a) *Movie Trailers* (b) *Cartoon Clips* (c) *Video Games* (d) *News Reports*

Figure 22: Three typical OLED screen power consumption profile of each video category (in mW, 1500 frames).

or continuous view moving. The time period between two successive scene transitions defines the scene length. In key frame selection step, I select the start, the end, and the other 8 random frames of every scene to analyze the motion features. As discussed in Section 4.1, the information of both current and previous frames is required to calculate the dynamic power consumption of the OLED screen. In power profiling step, the improved dynamic OLED power model is applied to translate each key frame sample into the OLED power consumption profile for the further analysis of power features.

Combing Eq. (3.2) and Eq. (4.2), the OLED screen power profile of a given m^{th} key frame in n^{th} scene can be calculated as:

$$F_n^m = \sum_{i,j=0}^{p,q} \left[P_{dynamic}^{i,j}(R) + P_{dynamic}^{i,j}(G) + P_{dynamic}^{i,j}(B) + \right] \tag{4.3}$$

Here $P_{dynamic}(R)$, $P_{dynamic}(G)$, $P_{dynamic}(B)$ are the improved dynamic power consumptions of the red, green, and blue OLED cells, respectively.

A given video stream x can be represented by a power profile sequence V_x, which includes the power consumptions of N scenes. For the scene $S_x^n (n = 1, ..., N)$, I use F_n^1 (or F_n^{start}), F_n^2, ... ,F_n^{10} (or F_n^{end}) to denote the OLED screen power profiles of the 10 sampled key frames. I then derive an OLED screen power profile sequence of each video stream as:

$$V_x = S_x^1, S_x^2, ..., S_x^N, \qquad S_x^n = F_n^1, F_n^2, ..., F_n^{10} \tag{4.4}$$

4.2.2.2 Temporal Motion Features (TMF) The camera motion, illumination, noise, shot, and scene of a video stream keep changing with ambient conditions. Thus, motion feature can be considered as an important characteristic of a video stream in time domain and significantly affects the power consumption of the OLED display [43]. In previous studies on video classification, the concept of Temporal Color Motion Energy (TCME) was introduced to describe motion features of a video [44, 45]. In this work, temporal motion features, which are distinctive between different video categories, are characterized by the OLED power profile. In [45], the authors proved that the motion energy of a video stream generally follows Gaussian distribution. Thus, based on the characterized OLED screen power profiles at scene and frame levels, I construct the temporal motion features at follows:

(1) *Overall Video Power Distribution (OVPD)*

As the power of each scene may vary dramatically, I extract the overall video power distribution (OVPD) from the average power consumption of each scene (with 10 sampled frames), i.e., $S'^{n}_{x} = \Sigma^{10}_{m=1} \cdot F^{m}_{n}/10$. The distribution of the temporal motion features across all the scenes of a video stream x can be measured by:

$$\mu^{O} = \frac{\sum_{n=1}^{N} S'^{n}_{x}}{N-1}, \qquad \sigma^{O} = \frac{\sum_{n=1}^{N} (S'^{n}_{x} - \mu_{O})^{2}}{N-1} \tag{4.5}$$

Here, μ^{O} and σ^{O} are the mean and the standard deviation of the OVPD, respectively, for video stream x. In other words, the OVPD of a video can be expressed by μ^{O} and σ^{O} as:

$$OVPD = \mu^{O}, \sigma^{O} \tag{4.6}$$

(2) *Inner-Scene Color Motion (ISCM)*

The variation of the OLED screen power consumption within each scene, denoted by Inner-Scene Color Motion (ISCM), is also an important character to describe the temporal motion feature of a video stream at scene level [38, 44]. As an example, Figure 22 shows that cartoon clips have a stationary background in each scene, resulting in very small inner-scene power variations. $Video\ games$, which track OLED screen records of video games, demonstrate much larger power variance within each scene because of continuous camera movement and frequent visual effects. The distribution of temporal motion features of the scene S^{n}_{x} can be extracted from the power profile of each frame as:

$$\mu^{I} = \frac{\sum_{m=1}^{10} F^{m}_{n}}{10-1}, \qquad \sigma^{I} = \frac{\sum_{m=1}^{10} (F^{m}_{n} - \mu_{O})^{2}}{10-1} \tag{4.7}$$

Here, μ^{I}_{n} and σ^{I}_{n} are the mean and the standard deviation of the OLED screen power consumption of each frame in S^{n}_{x}. In general, the ISCM of a video stream can be expressed as:

$$ISCM = \left\{(\mu^{I}_{1}, \sigma^{I}_{1}), (\mu^{I}_{2}, \sigma^{I}_{2}), ..., (\mu^{I}_{N}, \sigma^{I}_{N})\right\} \tag{4.8}$$

(3) *Cross-Scenes Color Motion (CSCM)*

The last TMF is the power consumption difference between the scenes in a video stream. For example, news reports have infrequent scene transitions. The display contents are often stationary and the power consumption difference between two adjacent scenes is generally low. Movie trailers, however, have much more frequent scene transitions and larger changes of the display content between two adjacent scenes, causing high power spike during scene transitions. Hence, I introduce Cross-Scenes Color Motion (CSCM) to describe the statistics of the power consumption difference between successive scenes as:

$$\mu_n^C = \frac{\sum_{n=2}^{N} \mid F_n^{Start} - F_{n-1}^{End} \mid}{N-1} \qquad \sigma_n^C = \frac{\sum_{n=2}^{N} (F_n^m - \mu_O)^2}{10-1} \tag{4.9}$$

Here $\mid F_n^{Start} - F_{n-1}^{End} \mid$ is the power consumption change between the $(n-1)^{th}$ and n^{th} scenes. μ_n^C and σ_n^C (2<n<N-1) are the mean and the standard deviation of the power changes of any two successive scenes. The CSCM of a video stream can be expressed as:

$$ISCM = \left\{(\mu_2^C, \sigma_2^C), (\mu_3^I, \sigma_3^I), ..., (\mu_{N-1}^I, \sigma_{N-1}^I)\right\} \tag{4.10}$$

4.2.2.3 Spatial Structure Features (SSF) Besides temporal motion features illustrated above, there are also spatial structure features for each video category. For instance, at the beginning of movie trailers, there is always a static green rating information lasting about 4∼5s. A stable power consumption of OLED display can be observed accordingly. Similarly, the logos shown at the beginning of news reports also consumes a constant power. Long stationary scenes over 30s, however, might exist in only certain games and news because of some video editing structure requirements or preferred colors and light tones. Compare to temporal motion features, spatial structure features could be more effective to reflect the distinctive power characters of some video categories [38, 46].

In this work, I identify several spatial structure features for video classification purpose, including static opening/ending information (i.e., $>$ 4 s); stationary long scene (i.e., $>$ 20 s); flashing scenes (i.e., $<$ 2s); and gradual scene change, whose SSIM value of adjacent scenes between 0.6 and 0.8 (usually $<$ 0.4 for a clear scene change); extremely low power (i.e., 50% scenes $<$ 100 mW); and extremely high power (i.e., 50% scenes $>$ 300 mW).

Table 4: Temporal Motion Features Analysis

Temporal Motion Feature	M	C	G	N
Overall Video Power Distribution avg. μ_O (mW)	96.2	361.4	125.6	221.2
Overall Video Power Distribution avg. σ_O	41.5	79.4	53.2	23.3
Inner-Scene Color Motion avg. μ_I (mW)	70.5	14.2	43.7	17.3
Inner-Scene Color Motion avg. σ_I	18.2	4.7	35.5	3.5
Cross-Scene Color Motion avg. μ_C (mW)	198.9	120.5	78.8	87.8
Cross-Scene Color Motion avg. σ_C	47.8	46.3	26.4	10.6

M: $Movie\ tralers$. C: $Cartoon\ clips$. G: $Video\ games$. N:$News\ reports$.

Table 5: Spatial Motion Features Analysis

Spatial Structure Feature	M	C	G	N
Static opening information ($>$ 4s)	88.4%	2.3%	7.2%	35.6%
Static ending information ($>$ 4s)	35.8%	1.5%	3.9%	37.4%
Stationary long scene (scene $>$ 20s)	0.7%	4.4%	35.4%	49.7%
Extremely low power (50% scene $<$ 100mW)	63.5%	0.8%	6.4%	0.5%
Extremely high power (50% scene $>$ 300mW)	1.4%	63.3%	2.5%	33.6%
Flashing scenes ($<$ 2s)	43.2%	20.5%	14.2%	7.0%
Gradual scene change (0.6 $<$ SSIM $<$ 0.8)	23.5%	7.8%	63.4%	6.4%

4.2.3 Power Feature based HMM Classifier

4.2.3.1 Power Feature Retrieval To have a better understanding on the statistics of these power features, I retrieve the power feature values based on a considerable volume of testing samples. For each category, $\sim$80 video streams were collected from official publication sources on $YouTube$ to guarantee the correctness of the category information, representative video format, and reasonable video quality. Based on the extracted power features of each video stream described

in Section 4.2.2, I can interpret the power profile of a video stream as representative characters of each video category. The statistical feature analysis results are summarized in Table 4 (temporal motion features) and Table 5 (spatial structure features), respectively.

Table 4 illustrates the mean and the standard deviation of the three temporal motion features proposed in Section 4.2.2. Due to space limit, only the average values of each parameter for all the video streams in each category are listed. The parameters of each category vary considerably, indicating distinctive power profile features. Although some categories have a few similar features, such as $movie\ trailers$ vs. $cartoon\ clips$ in OVPD, $cartoon\ clips$ vs. $news\ reports$ in ISCM, and news reports vs. video games in CSCM, none of the categories are similar in all the features. It conceptually proves that temporal motion features can effectively characterize a video stream's power profile.

Table 5 depicts the occurrence probability of each spatial structure feature in different categories. Some category-specific characters show up in the majority of the video streams from specific categories (e.g., 88.4% for static opening information in $movie\ trailers$) but with a low occurrence probability in other categories (e.g., 0.8% for extremely low power in cartoon clips).

4.2.3.2 HMM Classifier Construction

Traditional studies on video analysis and classification often rely on video features such as display content objects, color histogram, category information label, etc. Compare to these video features, the link between the power features and the category of a video may looks week. However, as I shall show in this section, using power features constructed in Section 4.2.2 can achieve reasonably high classification accuracy of video category by leveraging the proposed power feature based HMM (Hidden Markov Model) video category classifier.

HMM is expected to match an unknown video stream's power feature's (observation symbol) temporal sequences (observation states) to the transition probability matrix and generate the most likely category (model state) [39]. In our design, I build ten feature vectors composed of three temporal motion features and seven spatial structural features. Since the formats of various power features are different, I need to apply different policies to each feature to generate the probability matrix:

Spatial structure features can be transferred as the classification probability with video streams satisfying the conditions. Hence, they can be directly applied the HMM probability matrix. As described in Section 4.2.2, temporal motion features are pairs of mean and standard deviation. In general, a Pseudo 2D HMM is used to model such two dimensional data. However, Pseudo 2D HMMs nest two sets of HMMs, introducing significantly high design complexity [40]. Therefore, instead of using Pseudo 2D HMM, I transfer the pair sequence of the temporal motion features to a probability density function (PDF) of 2D Gaussian distribution to generate the classification probability. I also built three HMM probability matrix for all temporal motion features respectively. Following the above method, the HMM network used in the classifier can be trained based on the statistics of the power features of the characterized total 320 video streams. Hence I can determine each matrix's configuration and their relative weights. The proposed HMM classifier is depicted in $Algorithm$ 1.

Algorithm 1 *HMM Classifier Construction & Training*

***HMM Construction*:**

***model states*:**

$HMM^{ms}_{ovpd}=HMM^{ms}_{iscm}=HMM^{ms}_{cscm}=$ ('*Movie Trailers*', '*Cartoon Clips*', '*Video Games*', '*News Reports*').

***observation symbols*:**

HMM^{os}_{ovpd}=(*OVPD*'); HMM^{os}_{iscm}=(*ISCM*'); MM^{os}_{cscm}=(*CSCM*').

OVPD', *ISCM*', *CSCM*' is the 2D-Gaussian distribution probability based on *OVPD*, *ISCM* and *CSCM*, respectively.

HMM^{os}_{ssf}=(*SSF*').

SSF' is the classification probability transferred from occurrence probability of *SSF* as shown in *Table 2*.

***observation stages*:**

$HMM^{ot}_{ovpd}= HMM^{ot}_{ssf}$ =(*1*), only 1 value for each video stream;

HMM^{os}_{iscm}=(*g*), HMM^{os}_{cscm}(*g-1*), *g=5*.

g is the minimal scene change number in the video stream pool.

***HMM Training*:**

***Input*:** $V_i^n \in \{V^1(V_1{}^1,..., V_i{}^1),..., V^n(V_1{}^n,..., V_i{}^n)\}$, *i*=pool size of 80, *n*=4;

Each video has it power features analyzed as V_i^n-*OVPD*, V_i^n- *CSCM*, V_i^n-*ISCM* and V_i^n-*SSF*.

***Output*:**

$VCPr(V_x)=aHMM_{ovpd}(V_x)+bHMM_{ISCM}(V_x)+cHMM_{CSCM}(V_x)+dHMM_{ssf}(V_x)$

A random video stream, V_x's classification is calculated by *VCPr*(). It is composed of 4 HMM models for 1 set of spatial structural features, 3 temporal motion features. Their relative weights are *a, b, c, d*.

Figure 23: HMM classifier construction $Algorithm$ 1.

4.2.3.3 HMM Classifier Evaluation I measured the accuracy of the proposed HMM classifier using another 200 random video streams from the selected four categories. The classification re-

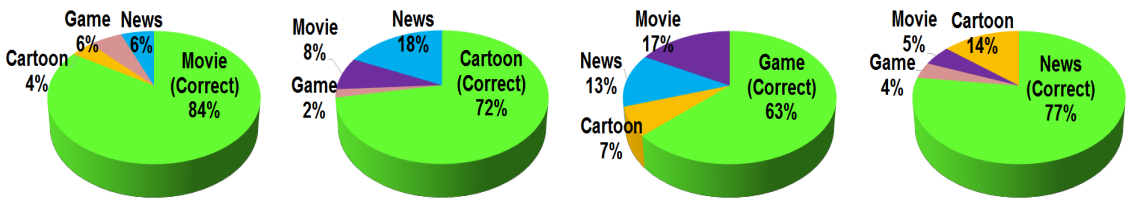

(a) *Movie Trailers* (b) *Cartoon Clips* (c) *Video Games* (d) *News Reports*

Figure 24: Power feature based HMM video classifier results, including the incorrect classification results.

sults are shown in Figure 24. The highest accuracy is achieved at movie trailers, in which 84% video streams are correctly classified. For *cartoon clips*, *video games* and *news reports*, the corresponding accuracies are 72%, 63%, and 77%, respectively. Figure 24. also shows the probability of classifying a video stream to a wrong category. The highest error rate occurs on cartoon clips, where 18% cartoon clips are wrongly classified as news reports, implying the similarity in the power characters of these two categories. Nonetheless, the results show that the video classification based on the OLED screen power characters can achieve a reasonably high accuracy, which can be utilized to guide the OLED power management without costly video content analysis.

4.3 DATUM IMPLEMENTATION AND EVALUATION

After the video classification information is obtained, I develop a video classification based dynamic tone mapping (DaTuM) scheme to optimize the power consumption of OLED screens: three DTM policies are designed for different video categories based on their power characters. For an unknown video, once its category is classified, the designated DTM policies are applied to achieve the maximized power saving with the minimized display quality degradation. In this section, I will introduce the working mechanisms of the proposed DaTuM scheme and its applications in OLED power management.

4.3.1 Power Optimization with DTM

Almost all display power management techniques are associated with display quality degradation. In LCD, for example, power saving can be achieved by dimming the backlights, incurring luminance losses [15, 30]. In dynamic voltage scaling (DVS) scheme of OLED screens, the displayed color is distorted by the degraded driving ability of OLED pixel drivers, hence, needs to be compensated by tuning the color value [47]. In LCD designs, DTM scheme was proposed to adjust the displayed color for power saving [18], resulting in inevitable display quality degradation. A popular criteria to evaluate the display quality is SSIM [27]: An SSIM in 1∼0.98, 0.98∼0.96, and 0.96∼0.94 represent high quality, medium quality, and low quality respectively. An SSIM below 0.94 means that there is phenomenal visual distortion that can be easily perceived by human vision.

A DTM scheme is generally composed of some policies to process an image or frame, such as *color remapping*, *saturation tuning*, and *hue tuning* [48, 31]. In the following, I present OLED-applicable DTM scheme derived from these 3 policies.

(1) *Dynamic color range mapping*: The objective of this policy is to lower pixels' luminance, i.e., mapping color range of the pixels with high luminance to a lower one using gamma correction. For instance, I set a pixel luminance threshold l, which is usually the average luminance of the pixels on the screen. When the luminance of a pixel exceeds l, the following algorithm will be triggered to remap the color range of the pixel:

$$\begin{aligned} When, \quad & \{max\left[C_{in}(R,G,B)\right] + min\left[C_{out}(R,G,B)\right]/2\} < l, \\ Then, \quad & C_{out}(R,G,B) = C_{in}(R,G,B)/X)^{\gamma}, X > 1, \gamma \sim 1.5. \end{aligned} \tag{4.11}$$

Here, C_{in}(*R, G, B*) and C_{in}(*R, G, B*) are the original and remapped RGB color value of a pixel, respectively. X is the gamma scaling parameter that is related to specific video category, γ is a coefficient around 1.5. Obviously, all the RGB color channels of the pixel will be affected by dynamic color range mapping.

(2) *Saturation tuning*: In HSV color space, the color is represented by Hue, Saturation and Value (or luminance). In particular, saturation describes how a pure color is mixed with white, which is introduced by other color channels. The goal of saturation tuning is to reduce the contributions from power-inefficient color components and enhance with power-efficient ones while still maintaining the overall luminance. The saturation-tuning algorithm can be expressed as:

$$
\begin{aligned}
When, \quad & max\left[C_{in}(R,G,B)\right] = R \; or \; G; \\
and, \quad & max\left[C_{in}(R,G,B)\right] - B > \Delta_s; \\
then, \quad & C_{out}(R' \; or \; G') \\
& C_{out}(B') = C_{in}(B)Y, \\
& C_{out}(R'orG') = C_{in}(R \; or \; G) - Y.
\end{aligned}
\tag{4.12}
$$

Here Δ_s is a preset RGB color difference, which is usually set to $\sim$60. Y is the color reduction amount related to the video category. For the OLED screen of Galaxy S3, blue is the most power inefficient color. Note that the power efficiency of colors varies with the OLED technologies.

(3) *Hue tuning*: Hue tuning can be used to minimize OLED power when display content is dominated by power-inefficient colors, e.g., movie trailers and video games. The corresponding algorithm can be expressed as [43, 30]:

$$
\begin{aligned}
When, \quad & max\left[C_{in}(R,G,B)\right] = B, \\
and, \quad & max\left[C_{in}(R,G,B)\right] - B > \Delta_h, \\
then, \quad & h = 60(RG)/\left\{B - min\left[S_{in}\right]\right\} + 240, \\
& h' = h - Z, \\
& C_{out} = HSVtoRGB(h', s, l).
\end{aligned}
\tag{4.13}
$$

Here h, s, l are the hue, saturation and luminance parameters for HSV color space, respectively. During hue tuning, I first calculate the hue parameters based on RGB values. If blue dominates the displayed color of an OLED pixel, I will turn the hue into green domain with coefficient Z, which is related to specific video category. The luminance and saturation of the pixel remain the same in this policy. HSVtoRGB() is the transfer function from HSV space to RGB space.

Figure 25 illustrates the effects of the above three policies in processing image $Lena$ on an OLED screen. The power saving ratio and SSIM visual quality evaluations are also included. The algorithms are performed at frame level with the same set of parameters over all pixels. Interestingly, although the same SSIM value is achieved under all three policies, the perceived visual effects on each image are quite different: In dynamic color range mapping, many visual details are lost by dimming the high-luminance pixels; the skewed color composition in saturation tuning makes the image virtually "redder" by reducing the white component; hue tuning directly turns the blue tone into the green tone, causing obviously distorted visual effects.

Figure 25: Different DTM policies' effect.

These three polices also achieve different power saving efficiency: In dynamic color range mapping, the contrast ratio of some areas is raised. It makes the picture looks more vivid, but with the lowest power saving efficiency. Meanwhile, hue tuning obtains the best power saving but the converted image looks strange. In practice I should carefully select appropriate DTM polices to balance visual quality and power saving efficiency.

4.3.2 Proposed DaTuM Scheme

4.3.2.1 From Power Features to DTM Scheme Temporal motion features of a video stream generate the OLED screen power variations inner and cross scenes. For instance, movie trailers generally have higher peak power and scene transition frequency than other categories. Also, flashing scenes with high-luminance contents have a power range very different from the average power consumption and often cause high cross-scene power variations. However, the flashing scenes, which often last only 1$\sim$2 seconds, usually generate very minimal impact on viewer's visual experience. Based on these temporal motion features, I may apply very aggressive dynamic color mapping to reduce the luminance of these flashing scenes while still maintaining an acceptable overall SSIM of the video streams.

Spatial structure features of a video stream often generate some category-specific characters of the OLED screen power profiles. I note that some similar power features may come from different mechanisms: In *movie trailers* and *video games*, for example, high power consumption is mainly introduced by the high-luminance components in their complex color composition, e.g., white.

Algorithm 2 *Common VC-DTM Policy Set Extraction*

Input: $V_i^n \in \{V^1(V_1^1,..., V_i^1),..., V^n(V_1^n,..., V_i^n)\}$, i=pool size of 80, n=4;
Eq(13)=A, Eq(14)=B, Eq(15)=C.
Output: VC-DTM Policies
DTMset=$\{X(X^1,...,X^n), Y(Y^1,...,Y^n), Z(Z^1,...,Z^n)\}$.

For each video category set V_i^n **do**
Sample video stream V_x into frames:
$V_i^n = \{S_i^1, S_i^2,..., S_i^N\}$, $S_i^n = \{F_n^1, F_n^2, ..., F_n^{10}\}$;
For each $F_n^1 \in S_i^n \in V_i^n$ **do**
Initialize X_i^n=1, Y_i^n =5, Z_i^n=100,
While $SSIM[A(F_i^n)] > 0.97$, X_i^n += 0.2;
While $SSIM[B(F_i^n)] > 0.97$, Y_i^n+=5;
While $SSIM[C(F_i^n)] > 0.97$, Z_i^n+=5;
End
$X^n = avg(X_1^n,..., X_i^n)$, $Y^n = avg(Y_1^n,..., Y_i^n)$, $Z^n = avg(Z_1^n,..., Z_i^n)$,
End
Return *DTMset.*

Figure 26: Common DaTuM Policy Set Extraction $Algorithm$ 1.

In *cartoon clips* and *news reports*, however, high power consumption is commonly introduced by bright power inefficiency colors in long static scenes, e.g., blue and purple. Different DTM policies can be selectively applied to different categories with the optimized trigger threshold while the tuning coefficients are adjusted to control the display quality.

In the following paragraphs, I will first present the common DaTuM policies and then discuss category-specific DaTuM policies.

4.3.2.2 Common DaTuM Policies DaTuM policies describe how specific DTM schemes are applied to each classified video category. In this work, I adopt those three common DaTuM policies discussed in Section 4.3.1 and configure their parameters for each video category. For each video category, I trained the applied DaTuM policy set on 80 video streams to achieve maximum power consumption with reasonable video stream quality. The threshold parameters of each DaTuM policy set are trained with different initial values and steps, which reflect the power features of the category. A relatively high video stream quality threshold, say, SSIM=0.97, is used to control the display quality degradation during training iterations. Any training result with a display quality worse than the threshold will be discarded. Theprocedure of common DaTuM policy set extraction is shown in *Algorithm 2.*

(a) Original *Video Game* Frame | *(b) Video Game* Frame *with less visual effect* | (c) Original *Movie Trailer Frame* | (d) Movie Trailer Frame with Saturation and Hue Tuning

Figure 27: Frames processing under common DaTuM policy set.

During the applications of DaTuM, I apply the trained DTM policy set to the whole video stream based on the classified or official category information. Note that the actual display quality of the video stream processed under the DaTuM policy set may be lower than the quality threshold used in the training process.

Figure 27 uses several examples to demonstrate the effectiveness of the common DaTuM polices. Figure 27(a) shows a video frame of a *video game* while Figure 27(b) shows the result after an aggressive dynamic color range map is applied. The bright visual effect is reduced and some details of the video frame become blurred. Also, saturation tuning enhances red color on the video frame and eliminates white component. The application of these DaTuM policies results in a 20.42% power saving with an SSIM of 0.974. Comparing Figure 27(c) and (d), an obvious hue tuning from blue to green is observed on the alien's face. Color saturation in the red and green background can be also observed. These effects bring in a 15.67% power saving with SSIM=0.948.

4.3.2.3 Category-specific DaTuM Policies Besides common DaTuM policies, I also propose two category-specific DaTuM policies to enhance the efficacy of DaTuM:

Color Remap: *Cartoons clips* and *news reports* may have very high average power consumption, e.g., 300mW in 50% of scenes. It is mainly because of extensive usage of power-inefficient colors, i.e., a bright blue background with white texts in news reports. Also, cartoons often use power-inefficient colors in a large area. Figure 28 (a) and (c) show two examples of *news reports* and *cartoons clips*, respectively. I applied hue tuning to these two examples by setting coefficient Z to 120 in Eq. (4.13). The processed results are shown in Figure 27 (b) and (d), respectively.

(a) Original *News Report* Frame | *(b) News Report* Frame *with Hue Tuning* | (c) Original *Cartoon Clip Frame* | *(d) Cartoon Clip* Frame *with Hue Tuning*

Figure 28: Frames with category specific DaTuM policies.

Many areas originally filled with bright blue are tuned into green. The power savings achieved in Figure 27 (b) and (d) are 14.47% and 11.53%, respectively. By specifying the color to be tuned, I avoid influencing the colors of certain objects that are sensitive to the viewer, e.g., human face. Although the colors of many areas are changed, the display quality is still retained at a reasonably high level, e.g., SSIM=0.942 (news),0.955 (cartoon), respectively.

Opening/Ending Dim: As described in Table 5, most movie trailers have a static scene in the video streams' opening and ending. When processing video streams form *movie trailers*, I directly set X to 3 in Eq. (4.11)for the first 4 seconds, which contain some general movie information, to make the whole screen darker. Similar strategy can be applied to other video streams with standard format or fixed content sequence.

4.3.3 Experiments and Discussion

The measured power savings and SSIM-based display quality of 150 video streams per video category when DaTuM is applied are summarized in Table 3 (denoted by HMM). The average power saving ratio is 17.80% while the highest power saving is achieved at *video games* (23.08%): the video streams of video games include almost all types of video features whose power can be effectively reduced by DTM. The lowest power saving occurs at movie trailers of which the original power consumption of every video stream has been already low. The average SSIM of all processed video streams is 0.96, which denotes medium display quality. However, the achieved levels of SSIM in each category vary insignificantly.

Table 6: Power Performance Evaluation

Evaluation	Classification	M	C	G	N	Avg.
Average Power Savng Ratio (%)	HMM	14.36	15.14	23.08	15.72	17.80
	Official	10.53	12.84	18.67	12.64	13.72
Average SSIM	HMM	0.9645	.9642	0.9706	0.9625	0.9696
	Official	0.9655	0.9640	0.9703	0.9574	0.964
Correlation	HMM	-0.515	-0.617	-0.622	-0.544	-0.575
	Official	-0.508	-0.610	-0.566	-0.535	-0.554

In general, a large power saving ratio is associated with high display quality degradation. The average correlation coefficient between power saving ratios and SSIM values of all video streams is -0.57, implying a considerably high correlation between power saving and display quality degradation. For comparison purpose, I also apply DTM scheme to the same video streams based on the official category information provided by the video streams themselves. Note that this information is only used to classify the category of the video streams but does not change the training process of the DTM policies. As shown in Table 6 (denoted by "Official"), the average power saving ratio of the DTM with official category information is only 13.72%, which is lower than that of DaTuM. This result indicates the slightly better power saving efficiency of DaTuM. It also implies that the official category classification is purely content-based but does not reflect the actual power features as accurately as our HMM classifier does. The average SSIM value of the DTM with official category information is 0.96, which is also slightly lower than that of DaTuM. It means that DaTuM can achieve better power saving efficiency and display quality control simultaneously than the DTM with official category information. I also observe a lower correlation coefficient (-0.55) between the power saving ratios and SSIM values of the DTM with official category information Note that a higher (absolute) value of the correlation coefficient represents better controllability of the trade-off between power saving and display quality (degradation).

The computation complexity of power management scheme is very crucial for timing-critical applications. The improvement on the power management efficiency is often followed by the

exponential increase in computation cost. In this research, I will explore the low-cost power management scheme that can fit into the timing constraints of real-time applications, such as the approximation on scene transition location and sub-optimal DVS/DTM scheme. I will also study the trade-offs between the power management efficiency and computation complexity in commercial mobile platforms.

4.4 CHAPTER 4 SUMMARY

In this work, I proposed a video classification based dynamic tone mapping (DaTuM) scheme for OLED screen power optimization. DaTuM is inspired from the similarity among the power features of the video streams from the same category. After identifying a series of OLED power features of video streams and developing a power feature-based HMM video classifier, I developed custom DaTuM policies sets designated to each video category to maximize OLED power saving with minimized display quality degradation. A mobile video player is also developed to realize DaTuM and used to perform the power measurement experiments. Experimental results show that DaTuM can achieve on average 17.8% OLED screen power saving, while maintaining a medium display quality. Detailed analysis shows that besides higher power saving, DaTuM also offers better controllability of the trade off between power saving and display quality compared to the DTM scheme with official category information and one state-of-the-art scheme.

5.0 OLED DISPLAY POWER OPTIMIZATION IN INTERACTION LEVEL

In previous Chapter 1, user interaction is also very important in the smartphone power consumption. Existing attempts for OLED power optimization have mainly focused on modifying the content that is shown on the display dur- ing the playback phase, requiring significant overhead in terms of image analysis and modification. While such methods are effective, these approaches overlook opportunities present during the camera recording phase, where utilization of already determined camera parameters could reduce or eliminate the image processing overhead. Hence, in this section I propose MORPh, a cross-layer optimization system for OLED. We first analyze three fundamental parameters extracted from the smartphone camera and their impact on OLED power consumption and visual quality. We then define corresponding metrics to assess power optimization potentials, and propose a set of algorithms that optimize camera recording to be more OLED friendly.

The rest of this chapter is organized as follows: Section 5.1 first gives the preliminary for the camera recording. Section 5.2 shows the power optimization schemes based camera recording. Section 5.3 shows the proposed interaction level OLED power optimization technique – mobile oled-friendly recording and playback system for low power video streaming (MORPh). Section 5.4 summarizes this chapter.

5.1 CAMERA RECORDING IN SMARTPHONE SYSTEM

Fig. 29 illustrates an overview of the camera processing flow in modern smartphones. Before the user even begins to capture an image or video, various auto-processing algorithms are continually analyze the scene in order to determine the camera parameters required for best quality. Parame-

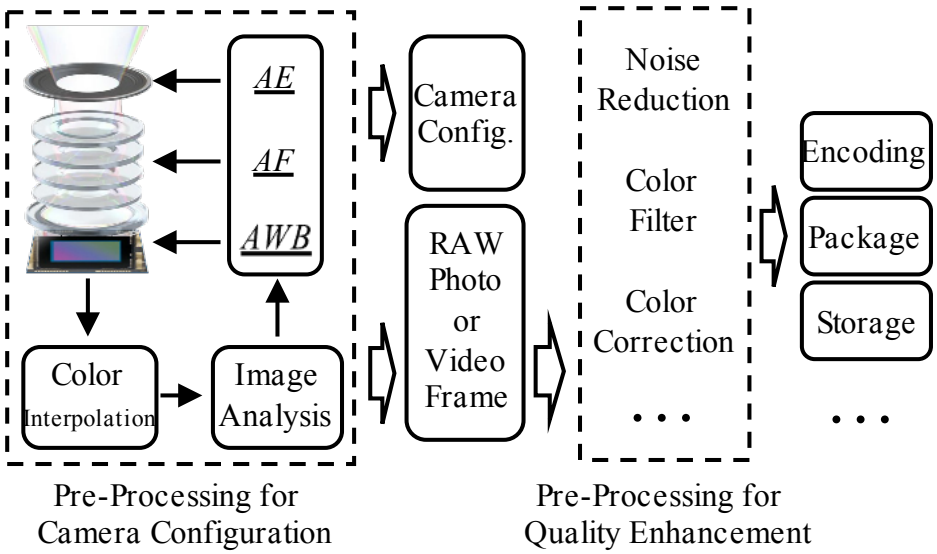

Figure 29: Smartphone Camera Processing Chain

ters determined in this manner include the aperture size, exposure time, and focal length. These parameters, in turn, affect features such as focus area, brightness, and color histogram of the final image. Image quality enhancements, such as noise reduction, color effect, color correction, and even high dynamic range (HDR), are also applied before final storage.

The parameters above, which are calculated during the recording phase, provide ideal support for OLED power optimization techniques. In this work, we examine three of the most fundamental camera preprocessing algorithms: *auto exposure* (AE), *auto focus* (AF), and *auto white balancing* (AWB).

5.1.1 Visual Quality in Camera Recording

In this work, the proposed MORPh technique used not only to modify power consumption of the OLED display, but also to improve perceived image quality. It is difficult to measure image quality quantitatively, especially with the naturally subjective nature camera recordings. In practice, many different image quality definitions have been suggested in order to effectively compare images [49, 50, 51, 52]. Since the HVS is most sensitive to image contrast ratio, in this work, we adopt *measure*

of enhancement (EME) as a method to quantify perceived image quality as a function of contrast distribution. The EME algorithm can be formulated as [52]:

$$EME_{\delta,\varepsilon,\zeta,k_1,k_2}(F) = \frac{1}{k_1 \times k_2} \sum_{n=1}^{k_2} \sum_{m=1}^{k_1} 20 \log \frac{I_{\max}^{w_{m,n}}(F)}{I_{\min}^{w_{m,n}}(F)}, \tag{5.1}$$

where the image f is transformed to F by processing methods of δ, ε, and ζ. The image is split into $k_1 \times k_2$ blocks, and in a single block $w_{m,n}$, $I_{\max}^{w_{m,n}}(F)$ and $I_{\min}^{w_{m,n}}(F)$ represent the maximum and minimum luminance intensity of the image F. In later parts δ, ε, and ζ will be defined as specific optimization processes. EME values of both F and f will be given as a ratio: the original frame's EME equals 1, and EME$>$1 indicates quality enhancement.

5.2 ANALYSIS FOR CAMERA METRICS & OLED PLAYBACK POWER CONSUMPTION

As presented above, the deep image processing which occurs during the camera recording phase may provide opportunities for OLED-specific optimization which can benefit future playback power consumption. In this section, three fundamental camera processing algorithms are analyzed from the perspectives of both OLED power consumption and user-perceived image quality.

5.2.1 AF for Focus Area Detection

AF algorithms determine the correct focal length required to clearly capture the image within the focus area. This is accomplished by dividing the current scene into multiple sample blocks and calculating the total contrast within each block. This is repeated as the camera lens sweeps through all the possible focal lengths. As the HVS is most sensitive to contrast, and as sharp, clear edges on objects cause high contrast values, the correct focal length is determined as the one which maximizes the contrast value within the current focus area.

The contrast distribution in the final image can be used to describe focus intensity, which is defined as the contrast value of each region in the image. The areas with the highest focus intensity

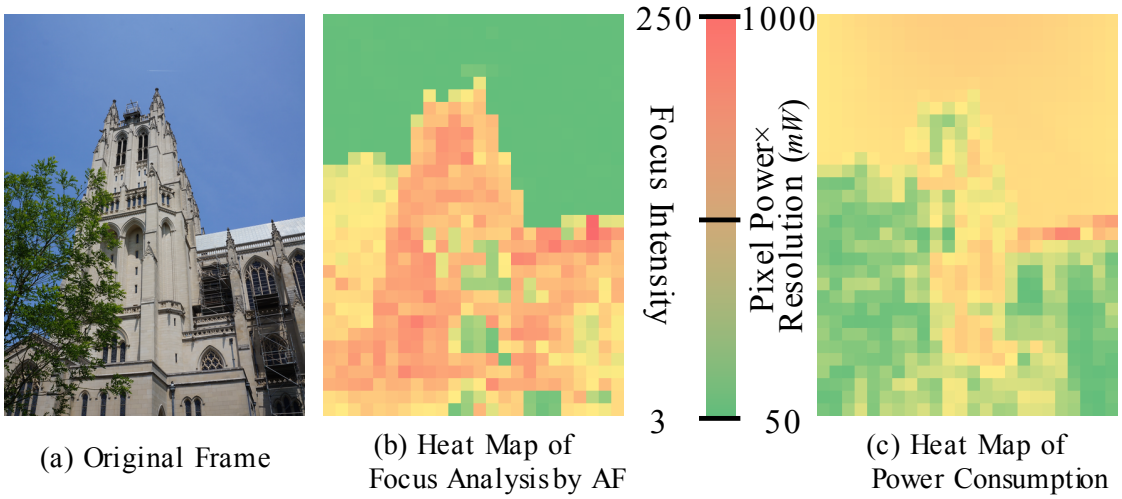

(a) Original Frame

(b) Heat Map of Focus Analysis by AF

(c) Heat Map of Power Consumption

Figure 30: Focus and Power Consumption Analysis with AF

are therefore the main focus area of the image. Given a block $w_(m,n)$ in frame image f, the focus intensity is formulated as:

$$FI_{AF}^{w_{(m,n)}} = I_{\max}^{w_{(m,n)}}[f^{w_{(m,n)}}] - I_{\min}^{w_{(m,n)}}[f^{w_{(m,n)}}] \tag{5.2}$$

Fig. 30(a) and (b) gives a frame and its focus intensity heat map analyzed via the AF process. We can see that contrast detection can effectively identify the regions of highest image detail and complexity, which are also the regions of the image a viewer is most likely to focus on. Based on the proposed OLED power model, a heat map of power consumption of the image is also generated and shown in Fig. 30(c). Compared to Fig. 30(b), the power consumption distribution on the OLED panel does not directly follow from the focus intensity map. As shown in previous works, the difference between areas of high focus intensity and areas of high power consumption can provide effective guidance for OLED local dimming schemes [53, 49, 50]. By utilizing an aggressive local dimming technique applied only to high power, but unfocused, areas, power consumption can be greatly reduced with little to no reduction in perceived quality.

From the analysis performed as part of AF, we can determine a metric to describe the reduction in OLED power consumption possible through applying local dimming to unfocused image areas:

$$Opt_{AF}^{LD} = \frac{\sum_{i=1}^{m} FI[w_{focus(i)}] \times \sum_{j=1}^{n} Power[w_{unfoc(j)}]}{\sum_{j=1}^{n} FI_{AF}[w_{unfoc(j)}] \times \sum_{i=1}^{m} Power[w_{focus(j)}]} \tag{5.3}$$

where $focus[]$ and $unfoc[]$ are the sequences of the focused and unfocused areas, and $FI_{AF}(w)$ and $Power(w)$ calculate the focus intensity and power consumption of selected block area.

In Section 5.3, Opt_{AF}^{LD} will be integrated with proposed optimization algorithm to guide quality retaining local dimming.

5.2.2 AE for Brightness Enhancement

In photography, exposure is used to coordinate the aperture size and exposure duration to adjust the overall brightness of the image:

$$EV = log_2(\frac{A^2}{E}) = 2log_2(A) - log(E) \tag{5.4}$$

where EV is the exposure value, A is the aperture size, and E is the exposure duration. Due to the lack of a dedicated ambient light analyzer on smartphones, the AE process is usually derived from the brightness of the focused area:

$$EV_{AE}^{focus} = EV_{pre} + \nu\{log_2[I_{pre}] - log_2[I^{w_{focus}}(f)]\} \tag{5.5}$$

where $I^{w_{focus}}(f)$ is the brightness of the focused area in frame image f, EV_{pre} and I_{pre} are preset constants for different scenarios, and ν is the scalar to adjust configurable EV_{AE}^{focus} range, which is $(-12, 12)$ for Android systems.

Fig. 31 illustrates the impact of the AE process on two photos, one taken during the day, and one at night. In the figure, the regions of highest focus intensity are annotated as yellow squares. It can be seen that while the AE process effectively increases the visibility of objects within the focus areas, it also significantly increase the overall brightness of the entire image. Moreover, the luminance histograms in Fig. 31(b) show that the AE process not only adjusts brightness, but also the brightness distribution. This is extremely inefficient for content which will be viewed on an OLED display, as the process shifts colors in the unfocused area towards less efficient values, consuming more power.

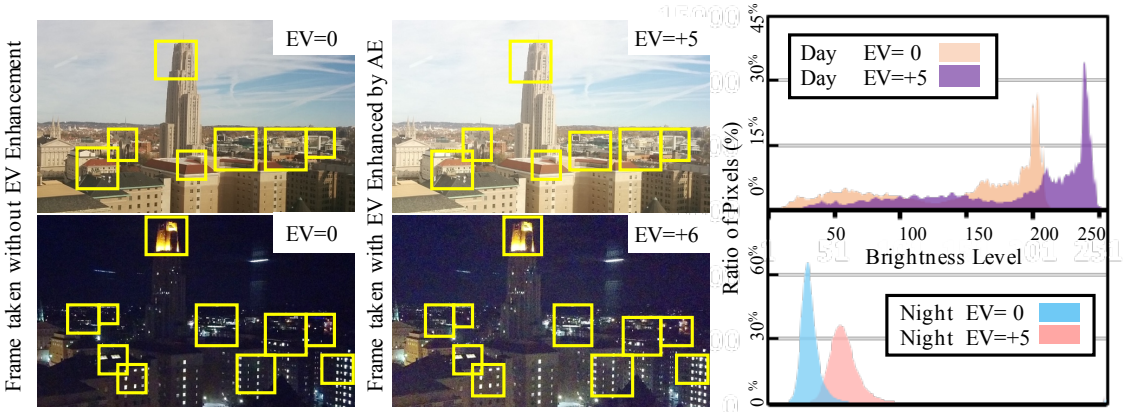

(a) EV's Impact on 2 Photos taken during Daytime and Night (b) Histograms of Frames

Figure 31: Exposure Effect on a Sample Image

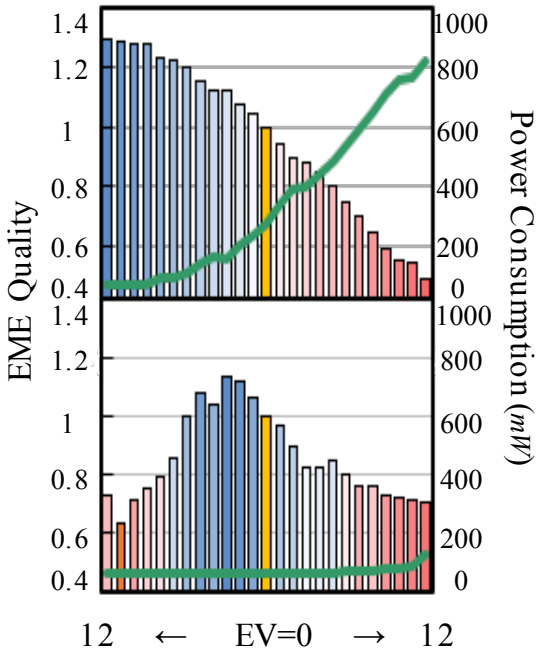

Figure 32: Quality and Power Analysis with AE

Different EV's are applied to the frames in Fig. 31(a) in order to examine the impact of EV on both OLED power consumption and perceived image quality, with Fig. 32 containing the results of the analysis. It can be seen that while an inverse correlation exists between power performance and EV, perceived image quality does not necessarily increase along with power consumption. In fact, the data indicates that when EV is pushed to the boundary values, a significant reduction in perceived image quality occurs. This is likely due to the loss of color information in large peripheral regions.

The analysis demonstrates that, the AE process does not currently consider the trade-off between power consumption and perceived image quality, when making modifications to an image or frame. Hence, an AE adjustment process specifically targeting the unfocused image area could likely be used to increase power performance with minimal impact on perceived image quality. To estimate the power overhead introduced by the current AE process, a reference EV_{AE}^{unfoc} for the unfocused area could be calculated, with $EV_{AE}^{focus}/EV_{AE}^{unfoc}$ as a power increment indicator:

$$Opt_{AE}^{RM} = \frac{EV_{AE}^{focus}}{EV_{AE}^{unfoc}} = \frac{EV_{AE}^{focus}}{EV_{pre}+\nu[log_2\frac{I_{pre}}{I^{w_{unfoc}}(f)}]} \tag{5.6}$$

In Section 5.3, Opt_{AE}^{RM} will be integrated with the proposed optimization algorithm to guide color range mapping. When over exposure happens in the unfocused area, color range mapping can be used to reduce the weight of power-hungry colors, as well as the related power consumption.

5.2.3 AWB for Color Correction

The various external light sources, such as sunlight, fluorescent lights, LED flash, and etc., each have a specific wavelength distribution $L(\lambda)$. When interacting with $T(\lambda)$, the reflected wavelength of an object's natural texture, the color perceived by the camera sensor is $S(\lambda) = L(\lambda)T(\lambda)$, and may not match the true color of the object. The goal of *white balance* (WB) is to apply a color transformation to a captured image such that the true color of objects in the scene are maintained. This is accomplished as:

$$S(\lambda)=\int_{400nm}^{700nm} WB(\lambda)L(\lambda)T(\lambda)d\lambda \tag{5.7}$$

where (400nm, 700nm) is the wavelength range of visible light and $WB(\lambda)$ is the color transformation function. Ideally, an external light analyzer can be utilized to precisely capture $L(\lambda)$.

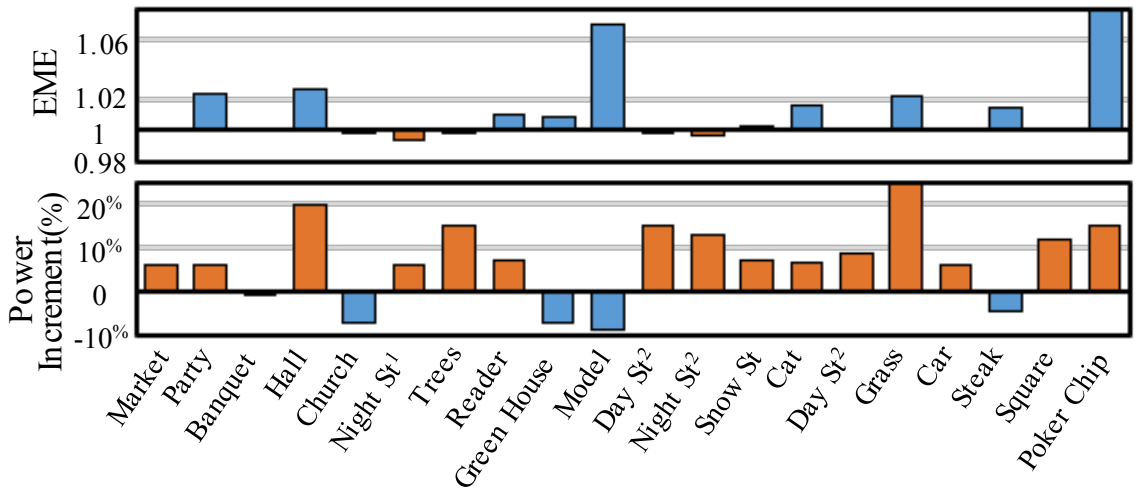

Figure 33: Power Analysis with AWB

However, due to the absence of such a component in existing smartphones, image analysis based on $WB_{AWB}^{(R,G,B)}$ modes is instead utilized to estimate the true $L(\lambda)$. One of the most widely used algorithms for this purpose, called *gray world*, functions as below:

$$WB_{AWB}^{(R)} = \psi \frac{G_{avg}}{R_{avg}}, WB_{AWB}^{(G)} = \psi, WB_{AWB}^{(B)} = \psi \frac{G_{avg}}{B_{avg}},$$
$$S_{AWB}^{(R,G,B)} = WB_{AWB}^{(R,G,B)} f^{(R,G,B)} \tag{5.8}$$

where R_{avg}, G_{avg}, B_{avg} are the average values of each RGB color component, ψ is a scene related constant, and $f^(R,G,B)$ is the pixel value in the frame. In this method, the color distribution is normalized according to green, the color to which the HVS is most sensitive.

Fig. 33 lists both the EME and power consumption analysis of 20 different video frame examples after the AWB process. The perceived image quality of most samples is improved. However, an increase in power consumption, averaging 10%, is widely present in the examples. This extra power is a result of the disproportionately high power consumption of the blue channel in the Galaxy S5 OLED display. Based on Eq. 5.8, a metric for power increment indication can be formulated as:

$$Opt_{AWB}^{TM} \approx (\frac{G_{avg}}{B_{avg}} - 1) \times P_B(B_{avg}) + (\frac{G_{avg}}{R_{avg}} - 1) \times P_R(R_{avg}) \tag{5.9}$$

To simplify Eq 5.9, P_B and P_A can be treated as liner functions $2\theta x$ and θx, as shown in Fig. 29. Then, Eq 5.9 can be formulated as:

$$Opt_{AWB}^{TM} \approx \theta(3G_{avg} - 2B_{abg} - R_{avg}) \tag{5.10}$$

where, if $3G_{avg} - 2B_{avg} - R_{avg} > 0$, a power increment caused by AWB will be introduced.

In Section 5.3, Opt_{AWB}^{TM} will be integrated with proposed optimization algorithm to guide dynamic tone mapping. When Opt_{AWB}^{TM} is big enough, the value increment in blue channel should be well controlled to prevent considerable extra power.

5.3 MORPH: MOBILE OLED-FRIENDLY RECORDING AND PLAYBACK SYSTEM FOR LOW POWER VIDEO STREAMING

Based on the analysis in Section 5.2, three metrics are proposed corresponding to three fundamental camera algorithm. In this section, the propose optimization system, *MORPh*, is derived from metrics and the implantation details will also be presented.

5.3.1 Optimization Algorithms in MORPh

5.3.1.1 AF Guided Local Dimming As mentioned in Section 5.2, Opt_{AF}^{LD} is proposed to assess the power optimization potential achieved by local dimming method.

The algorithm is shown in Figure 34, Opt_{AF}^{LD} is proposed to assess the power optimization potential achieved by local dimming method. The algorithm is shown in Figure 34.

In Algorithm 34, Opt_{AF}^{LD} is used as an switch for the local dimming process, and $Opt_{AF^{LD}} > 1$ shows that more energy is consumed on the unfocused areas. Based on the focus intensity distribution provided by the recording phase, unfocused areas are selected for down-scaling process. Rather than applying singable scalar, the dimming process is achieved by gamma. As shown in Algorithm 34, Opt_{AF}^{LD} is used as gamma correction parameter associated with a scale of $\gamma > 1$ for further adjustment. When $\gamma \times Opt_{AF}^{LD} > 1$, the gamma correction scales down the pixel value, while the peak value is maintained, and the histogram further extended into lower value range. Hence, the contrast ratio is further enhanced as well as perceived image quality.

Algorithm 1 AF Guided Local Dimming

procedure $MORPh_{AF}(f, FI_{AF^{w_{(m,n)}}}, Opt_{AF}^{LD})$
  Camera Auto Focus Detection
  $focus[], unfoc[] \leftarrow FI_{AF^{w_{(m,n)}}}$ ▷ Focus Distribution
  $Opt_{AF}^{LD} \leftarrow Eq.(5)$
  while $Opt_{AF}^{LD} > 1$ **do**
    for $w_{(m,n)}^{R,G,B} \in unfoc[]$ **do** ▷ Local Dimming
      $new - w_{m,n}^{R,G,B} \leftarrow 255 \times (\frac{w_{m,n}^{R,G,B}}{255})^{\frac{1}{\gamma \times Opt_{AF}^{LD}}}$
  return $new - w_{(m,n)}^{(R,G,B)}$

Figure 34: AF Guided Local Dimming

5.3.1.2 AE Guided with Color Range Mapping From the Eq. 5.6, two camera AE processes targeting both focused and unfocsed areas and generate Opt_{AE}^{RM}, which is used to assess the extra power consumption introduced by AE. When $Opt_{AE}^{RM} > 1$, the AE level that the focus areas require is higher than the unfocused one. Hence over exposure might happen to the unfocused area extra power consumption occurs during AE process. Given Opt_{AE}^{RM} and the camera's actual EV configuration parameter, the luminance intensity relationship of both focused and unfocsed areas can be calculated as:

$$\frac{I^{w_{unfoc}}}{I^{w_{focus}}} = 2^{\frac{(Opt_{AE}^{RM}-1)}{Opt_{AE}^{RM}} \times \frac{EV_{AE}^{focus}}{\nu}} \tag{5.11}$$

During the AE process, to prevent the over exposure of the unfocused area, the color range of $I^{w_{unfoc}}$ is remapped to $I^{w_{focus}}$, to maintain $Opt_{AE}^{RM} = 1$. The translation range $[\eta, \mu]$ is calculated from Eq. 5.11. Since the peak value of the unfocused area is reduced, the translation vector is extended in low color range to enhance the contrast ratio. The algorithm is shown in Figure 35.

Algorithm 2 AE Guided with Color Range Mapping

procedure $MORPh_{AE}(f, EV_{AF}^{focus}, Opt_{AE}^{RM})$
    Camera Auto Exposure Analysis for focused area.
    Camera Auto Exposure Analysis for unfocused area.
    $Opt_{AE}^{RM} \leftarrow Eq.(8)$
    if $Opt_{AE}^{RD} > 1$ **then**
        $\frac{I^{w_unfoc}}{I_{w_focus}} \leftarrow Eq.(13)$
        $\mu \leftarrow -(I^{w_{unfoc}} - I^{w_{focus}})$
        $\eta \leftarrow \mu \times (\frac{1}{2})^{\frac{1}{2.2}}$ ▷ Range Mapping
        $new - I^{w_{unfoc}} \leftarrow$ translated with $[\eta, \mu]$
return $new - I^{w_{unfoc}}$

Figure 35: AE Guided with Color Range Mapping

Algorithm 3 AWB Enhancement with Color Tone Mapping

procedure $MORPh_{AWB}(f, EV_{AE}^{focus})$
    Camera Auto White Balance
    $S_{AWB}^{(R,G,B)} \leftarrow Eq(10)$
    $Opt_{AWB}^{TM} \leftarrow Eq.(12)$
    if $Opt_{AWB}^{TM} > 0 \& G_{avg} > B_{avg}$ **then**
        $f^{(B)} \leftarrow S_{AWB}^{(B)} \times \frac{B_{avg}}{G_{avg}}$ ▷ Color Tuning for Blue
        $h^{(B)} \leftarrow f^{(B)} \times \frac{B_{avg}+G_{avg}}{2G_{avg}}$
        $f^{(R)} \leftarrow S_{AWB}^{(R)} \times \frac{R_{avg}}{G_{avg}}$ ▷ Color Tuning for Red
        $h^{(R)} \leftarrow f^{(R)} \times \frac{R_{avg}+G_{avg}}{2G_{avg}}$
        $h^{(G)} \leftarrow f^{(G)}$
    $new - f_{(i,j)}^{(R,G,B)} \leftarrow h^{(R,G,B)}$
return $new - f_{(i,j)}^{(R,G,B)}$

Figure 36: AWB Enhancement with Color Tone Mapping

5.3.1.3 AWB Enhancement with Color Tone Mapping

AWB process is supposed to balance the image spectra distribution against the influence. However, due to OLED's specific power model as shown in previous section, when $Opt^{TM}_{AWB} > 0$, extra power is introduce due to the augment of power-hungry color channels. To make AWB OLED power friendly, color tone mapping is utilized to enhance AWB from the power perspective as shown in Figure 36.

In Figure 36, when $Opt^{TM}_{AWB} > 0$, the white balancing is re-tuned with less aggrieve value augment in power-hungry channels.

5.3.2 System Implementation of MORPh

The proposed algorithms are integrated as a OLED power friendly recording and playback system, namely MORPh. It's implemented with Samsung Galaxy S5. The algorithms mentioned covering camera recording configuration and OLED power optimizations are implemented on Andriod 4.4.2 platform and Android Camera API (level 20), as shown in Fig. 37 In the MORPh two schemes are integrated for different recording and playback requirement: grated as a OLED power friendly recording and playback system, namely MORPh. It's implemented with Samsung Galaxy S5. The algorithms mentioned covering camera recording configuration and OLED power optimizations are implemented on Andriod 4.4.2 platform and Android Camera API (level 20), as shown in Fig. 37 In the MORPh two schemes are integrated for different recording and playback requirement:

cMORPh: In cMORPh scheme, the MORPh application works as a standalone camera recorder. As long as the video frame is captured, the proposed optimization will be directly applied, and the final video stream is only for Samsung Galaxy S5 or similar devices. However, during the recording phase, possible computation delay are tolerable, leaving no further computation load for the playback phase.

pMORPh: In pMORPh scheme, the MORPh application also works a player. During the camera recording, rather than directly change the captured video content, a separate file is generated to record the camera parameters, optimization metrics , focus intensity distribution and other related information. The content optimization only occurs until playback phase. This scheme can benefit more device configurations by retaining the original video content. However, a inter-

Figure 37: Experiemnt Setup with MORPh on Galaxy S5

framecomputation load is restricted according to different frame rate, preventing possible real-time performance failure. In next section detailed evaluation will be presented.

5.3.3 Optimization Algorithms in MORPh

5.3.3.1 Experiment Setup The indoor experiment setup is shown in Fig 37. To guarantee constant references for the captured video streams, all experimental subjects in this section are recorded via the MORPh application on Samsung Galaxy S5. 40 video stream samples are evaluated with different external light source conditions.

5.3.3.2 Performance with Camera Metrics In this work, three metrics are proposed, *i.e.*, Opt_{AF}^{LD}, Opt_{AE}^{RM}, and Opt_{AWB}^{TM}. These three meters doesn't only describes the impact of camera's configuration parameters' on the power consumption but also guided the further OLED specific optimization. Fig. 38 shows the correction features of the metrics. Opt_{AF}^{LD} describes the discordance between the focus intensity and power distribution, and indication the power saving potential utilizing local dimming, which has correlation value of $R^2 = 0.4728$. Meanwhile, Opt_{AE}^{RM} with $R^2 = 0.4866$shows that AF process based on the focus area might introduce significant power

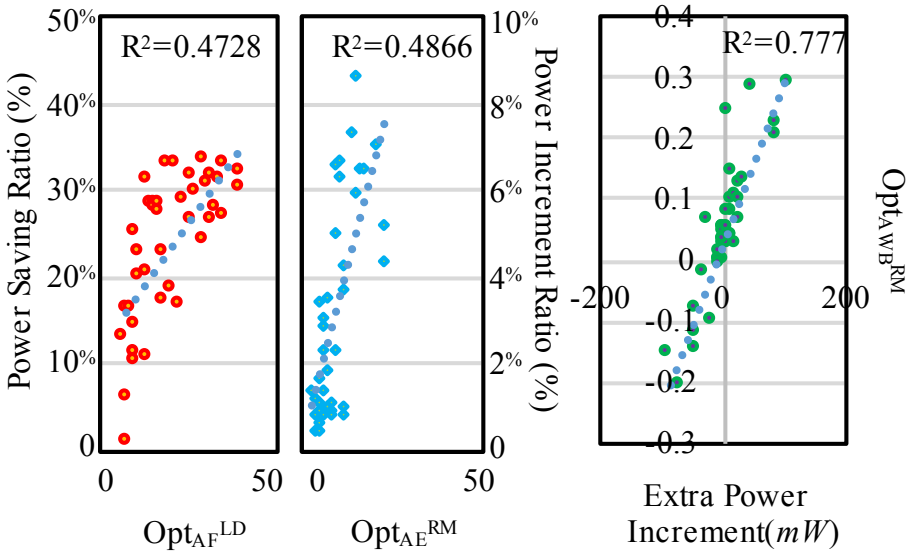

Figure 38: Power Consumption and Perceived Video Quality Performance Evaluation with MORPh

increment as much as 10%. The power increment caused by AWB can be perfectly predicted by Opt_{AWB}^{TM} with correlation value of $R^2 = 0.7768$.

5.3.3.3 Performance with MORPh In the experiment, four sets of power consumption performance of 40 video streams are included for the power consumption comparison, including the original video stream, the video stream captured by unoptimized Android camera and two MORPhs schemes. In Fig. 39, the power consumption of different process approaches are shown. According the power model, the original video stream has the biggest power consumption. When capture by the smartphone camera, high brightness components are lost and the EME quality is defected by 4%∼7%. An optimal power saving performance can be observed when using the MORPh application. Comparing the playback phase of cMORPh, which has optimized video stream ready for playback, the power saving ratio achieved is as high as 39%. Meanwhile, due to the contrast compensation during the optimization phase, the video quality is maintained at a range of -4.230%∼0.375% video quality. Moreover, the display power consumption difference be-

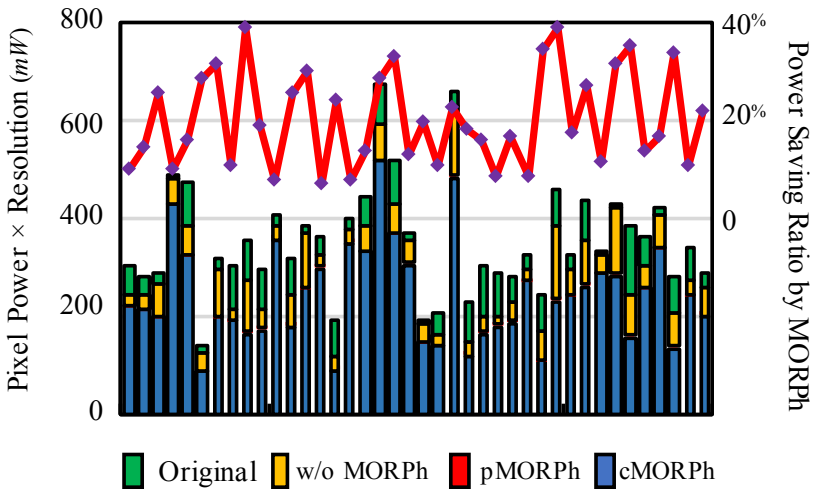

Figure 39: A Set Frame Examples for Different Process Approaches

tween the two MORPh schemes are hardly perceived. During the application experiment pMORh is tested under two different frames of 15fps and 30fps. However, by analysis the video frames decoded by pMORPh scheme, only few frames missed full optimization process, showing power consumption difference less than 10mW which is totally tolerable considering other interference inside of the smartphone system.

5.4 CHAPTER 5 SUMMARY

In this work, a low power optimization system, *i.e.* MORPh, is proposed. It works on both camera recording phase and video stream playback phase, and can provide real-time crossing-layer power optimization for OLED display on smartphone. Specifically, MORPh utilizes the digital camera configuration metrics as optimization index, and derives a set of corresponding optimization algorithms additional to the image processing through camera recording phase. During the playback phase, the video stream recorded with MORPh are enhance with have significant performance improvement in both power efficiency and HVS visual quality. MORPh is also implemented as a

practical Android application on Samsung Galaxy S5. And a series experiments are conducted to evaluate its performance. The experiment result over 50 video streaming show that MORPh can achieve significant power reduction of 20.3% on average. Meanwhile, evaluated by *EME*, the video quality is well retained., which benefit form the contrast enhancement in MORPh optimization.

6.0 CONCLUSION AND FUTURE WORK

6.1 DISSERTATION CONCLUSION

Smartphones have emerged as the most popular and frequently used platform for the consumption of multimedia. Following the rapid growth of application number and the explosion of cellular network bandwidth, high power consumption and limited battery capacity remain as the major challenges in smartphone designs. Therefore, lots of researches are made to characterize and optimize the smartphone power performance.

However, the existing research approaches on smartphone power characterization generally ignore the impact from the components' varying performance in different applications, as well as users' behavior during the practical usage. Hence, the power optimization techniques in modern smartphone are inflexible to adapt to different application scenarios and user behaviors.

In Chpater 2, I first proposed a new smartphone power consumption characterization and analysis approach – "SEER", which was associated with both user ethological and smartphone evolutionary perspectives. The real-time power consumption is measured with a set of the most popular applications on different generations of Samsung Galaxy smartphones. And deep analysis is made to find how each smartphone component is utilized in different applications, and how the users' daily usage patterns impact on final energy consumption. The experiments show that, some traditional power hungry components, such as Wi-Fi and CPU, actually consume much less energy in practical daily usage. Meanwhile, OLED display panel is still the biggest power consumer in the whole smartphone system; even it's considered the most promising low power display technology.

In Chapter 3, I further proposed a set of dynamic power optimization techniques for OLED display, balancing the real-time power performance and the user visual perception experience. In this chapter, the optimization take place in the hardware level, especially with the OLED driver

circuit. A DVS-friendly driver circuit and peripheral driver system was proposed. Then, I proposed an optimal DVS optimization method to manage the power consumption of OLED panels in video stream applications. Two optimization steps are applied for the real-time power saving, namely spatial supply voltage optimization and temporal supply voltage optimization. They are analyzed and implemented to guarantee the real-time video quality while receiving the minimal energy consumption. The experimental results on fmy typical test benches show that comparing to conventional global DVS solution, my technique saves 19.05% 49.05% OLED power on average while maintaining a high display quality (SSIM ¿ 0.98). Such a system is named DiViSi, which can be effectively save the power consumption with slight hardware modification.

However, not all the marketed smartphones can benefit from the hardware modification. In Chapter 4, I proposed a video classification based dynamic tone mapping (DaTuM) scheme for OLED screen power optimization. DaTuM is inspired from the similarity among the power features of the video streams from the same category. After identifying a series of OLED power features of video streams and developing a power feature-based HMM video classifier, I developed custom DaTuM policies sets designated to each video category to maximize OLED power saving with minimized display quality degradation. A mobile video player is also developed to realize DaTuM and used to perform the power measurement experiments. Experimental results show that DaTuM can achieve on average 17.8% OLED screen power saving, while maintaining a medium display quality. Detailed analysis shows that besides higher power saving, DaTuM also offers better controllability of the trade off between power saving and display quality compared to the DTM scheme with official category information and one state-of-the-art scheme.

Based on the understanding of the OLED optimization from both software and hardware perspectives, I took the optimization a further step to the user interaction oriented optimization. In Chapter 5, a low power optimization system, *i.e.* MORPh, is proposed. It works on both camera recording phase and video stream playback phase, and can provide real-time crossing-layer power optimization for OLED display on smartphone. Specifically, MORPh utilizes the digital camera configuration metrics as optimization index, and derives a set of corresponding optimization algorithms additional to the image processing through camera recording phase. During the playback phase, the video stream recorded with MORPh are enhance with have significant performance improvement in both power efficiency and HVS visual quality. MORPh is also implemented as a

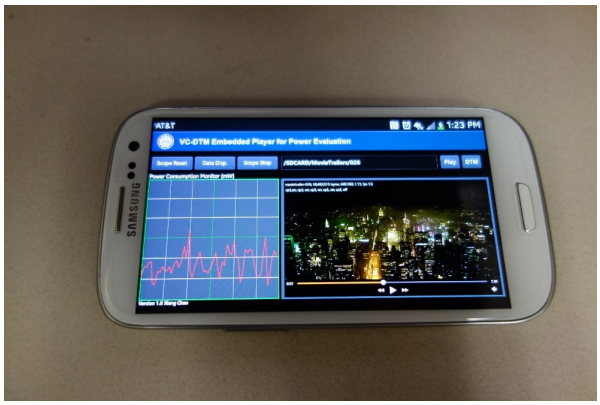

Figure 40: A DaTuM integrated android video player.

practical Android application on Samsung Galaxy S5. And a series experiments are conducted to evaluate its performance. The experiment result over 50 video streaming show that MORPh can achieve significant power reduction of 20.3% on average. Meanwhile, evaluated by *EME*, the video quality is well retained., which benefit form the contrast enhancement in MORPh optimization.

6.2 FUTURE WORK

In my present work, I have multiple approaches for smartphone energy analysis (from user ethological and smartphone evolutionary aspect), and different layers of OLED power optimization (application, hardware and system). Although in my OLED power optimization works, I am associating different layers of optimization in the same platform scenario of an Android system, I still lack lots of implementation work to do to release analysis and optimization techniques to end users for evaluation and feedback.

So, implementation is one of the very important task in the future work. I hope I can surmise and package my proposed analysis and optimization work into plantable libraries and integrate them in Android system: 1) “SEER” smartphone power library. I am aiming to built a smartphone power library on practical smartphone devices. It’s supposed to collect accuracy smartphone com-

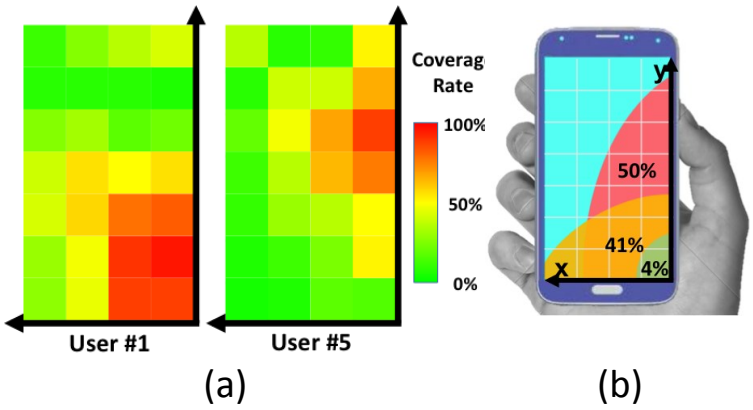

Figure 41: Finger operation behavior methodology: (a) Screen division and finger movement coverage, (b) Screen coverage heat maps from two users.

ponents models on different smartphones and collect users' Apps preference and usage behavior pattern to generate customized smartphone energy optimization scheme. 2) OLED power optimization scheme library. Similarly, I am also packaging my OLED related work into an integrated Android system support. I hope I can release a set of OLED power-friendly scheme library for the smartphone to share with power researcher and industry designer. Right now, I have already had some prototype application demos on Android smartphone. One example is a DaTuM integrated Android video player as shown in Fig. 40. I integrated my DaTuM technique into open smyce VLC player.

Also, I still have some new ideas to be verified and implemented. For the future work directions, I am going to further leverage the user interaction's impact on the practical smartphone power application. And I will focus on the research scope 2 to design dedicated smartphone Apps and system modules for high-reliable and high-performance power optimization.

For example, I am working on another OLED power optimization work with further user interaction study. Techniques such as local dimming are proposed to further reduce the power consumption of OLED screen, but it is hard to decide which part of the screen could be dimmed, and

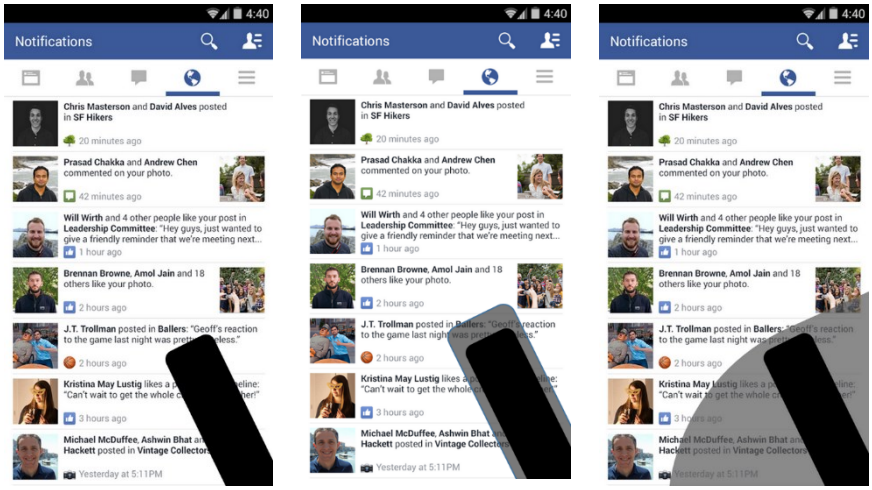

Figure 42: Different FingerShadow local dimming policy examples.

it often results in compromised user experience. Intuitively, as shown in 41, when a user interacts with a smartphone via the touch screen, the screen areas covered by the users fingers and even some of the neighboring areas could be safely dimmed.For example, the coverage ratios of the three patterns, shown in Fig. 41(a), are about 50%, 41% and 4%, respectively, and two user's finger action coverage maps are shown in Fig. 41(b).Thus, I propose FingerShadow, a new technique which does local dimming for the screen areas covered by user fingers to save more power, without compromising the user visual experience. I have studied 10 users touch interaction behaviors and found that on average 11% of the screen were covered by fingers. For these 10 users, I estimate that Finger-Shadow can achieve 5.07%∼22.32%, averaging 12.96%, with negligible overhead. In this work, I will also release correlated practical smartphone applications to end users for evaluation as shown in Fig. 42.

6.3 RESEARCH SUMMARY AND INSIGHT

In my PhD career, I mainly worked on the smartphone platform and the OLED display platform. Both of these two topics have demonstrated great potential in next-generation computing and interaction systems. In this dissertation, I demonstrate my understanding on smartphone system mechanism, power consumption, display system, and user interaction. I believe that, in coming age of virtual realization and augmented realized era, the display and related computing will continuous show their potential in both academia research and industry market.

BIBLIOGRAPHY

[1] J. Jacobs, D. Hente, and E. Waffenschmidt, "Drivers for oleds," in *Proc. of the 42nd Industry Applications Society Annual Meeting*, ser. IAS '07, Sep 2007, pp. 1147–1152.

[2] N. Balasubramanian, A. Blasubramanian, and A. Venkataramani, "Energy consumption in mobile phones: A measurement study and implications for network applications," in *Proc. of the 9th Internet Measurement Conference*, ser. IMC '09, 2009, pp. 280–293.

[3] N. Thiagarajan, G. Aggarwal, A. Nicoara, D. Boneh, and J. P. Singh, "Who killed my battery?: Analyzing mobile browser energy consumption," in *Proc. of the 21st International Conference on World Wide Web*, ser. WWW '12, 2012, pp. 41–50.

[4] C. Yoon, D. Kim, W. Jung, C. Kang, and H. Cha, "Appscope: Application energy metering framework for android smartphones using kernel activity monitoring," in *Proc. of the 2012 USENIX Annual Technical Conference*, ser. USENIX ATC '12, 2012, pp. 36–36.

[5] L. Zhang, B. Tiwana, Z. Qian, Z. Wang, R. P. Dick, Z. M. Mao, and L. Yang, "Accurate online power estimation and automatic battery behavior based power model generation for smartphones," in *Proc. of the 8th International Conference on Hardware/Software Codesign and System Synthesis*, ser. CODES/ISSS '10, 2010, pp. 105–114.

[6] A. Carroll and G. Heiser, "An analysis of power consumption in a smartphone," in *Proc. of the 2010 USENIX Annual Technical Conference*, ser. USENIX ATC '10, 2010, pp. 21–21.

[7] F. R. Dogar, P. Steenkiste, and K. Papagiannaki, "Catnap: Exploiting high bandwidth wireless interfaces to save energy for mobile devices," in *Proc. of the 8th International Conference on Mobile Systems, Applications, and Services*, ser. MobiSys '10, 2010, pp. 107–122.

[8] J. Liu, B. Priyantha, T. Hart, H. S. Ramos, A. A. F. Loureiro, and Q. Wang, "Energy efficient gps sensing with cloud offloading," in *Proc. of the 10th Embedded Network Sensor Systems*, ser. SenSys '12, 2012, pp. 85–98.

[9] T. K. Times, "Samsung, lg in legal fight over brain drain," 2010. [Online]. Available: http://www.koreatimes.co.kr/www/news/biz/2010/07/123_69626.html

[10] W. Graupner, C. M. Heller, A. P. Ghosh, and W. E. Howard, "High-resolution color organic light-emitting diode micro-display fabrication fethod," in *Proc. of State of the Photonics Industry*, ser. SPIE '10, vol. 4207, 2000, pp. 11–19.

[11] G. Gustafsson, Y. Cao, G. M. Treacy, F. Klavetter, N. Colaneri, and A. J. Heeger, "Flexible light-emitting diodes made from soluble conducting polymers," *Nature*, vol. 357, pp. 477–479, Jun 1992.

[12] D. Shin, Y. Kim, N. Chang, and M. Pedram, "Dynamic voltage scaling of oled displays," in *Proc. of the 48th Design Automation Conference*, ser. DAC '11, 2011, pp. 53–58.

[13] M. Dong, Y.-S. K. Choi, and L. Zhong, "Power-saving color transformation of mobile graphical user interfaces on oled-based displays," in *Proc. of the 2009 International Symposium on Low Power Electronics and Design*, ser. ISLPED '09, 2009, pp. 339–342.

[14] A. Iranli, W. Lee, and M. Pedram, "Hvs-aware dynamic backlight scaling in tft-lcds," *IEEE Trans. on Very Large Scale Integrated System*, vol. 14, no. 10, pp. 1103–1116, Oct 2006.

[15] W.-C. Cheng and M. Pedram, "Power minimization in a backlit tft-lcd display by concurrent brightness and contrast scaling," *IEEE Trans. on Consumer Electronics*, vol. 50, no. 1, pp. 25–32, Feb 2004.

[16] X. Chen, J. Zeng, Y. Chen, W. Zhang, and H. Li, "Fine-grained dynamic voltage scaling on oled display," in *Proc. of the 17th Asia and South Pacific Design Automation Conference*, ser. ASP-DAC '12, Jan 2012, pp. 807–812.

[17] M. Dong and L. Zhong, "Chameleon: A color-adaptive web browser for mobile oled displays," in *Proc. of the 9th International Conference on Mobile Systems, Applications, and Services*, ser. MobiSys '11, 2011, pp. 85–98.

[18] A. Iranli and M. Pedram, "Dtm: Dynamic tone mapping for backlight scaling," in *Proc. of the 42nd Design Automation Conference*, ser. DAC '05, 2005, pp. 612–617.

[19] M. Dong, Y.-S. K. Choi, and L. Zhong, "Power modeling of graphical user interfaces on oled displays," in *Proc. of the 46th Design Automation Conference*, ser. DAC '09, 2009, pp. 652–657.

[20] N. Eagle and A. Pentland, "Reality mining: Sensing complex social systems," *Personal Ubiquitous Computer*, vol. 10, no. 4, pp. 255–268, Mar 2006.

[21] H. Falaki, R. Mahajan, S. Kandula, D. Lymberopoulos, R. Govindan, and D. Estrin, "Diversity in smartphone usage," in *Proc. of the 8th International Conference on Mobile Systems, Applications, and Services*, ser. MobiSys '10, 2010, pp. 179–194.

[22] C. Shepard, A. Rahmati, C. Tossell, L. Zhong, and P. Kortum, "Livelab: Measuring wireless networks and smartphone users in the field," *SIGMETRICS Performance Evaluation Review (PER)*, vol. 38, no. 3, pp. 15–20, Jan 2011.

[23] A. Rahmati, C. Tossell, C. Shepard, P. Kortum, and L. Zhong, "Exploring iphone usage: The influence of socioeconomic differences on smartphone adoption, usage and usability," in *Proc. of the 14th International Conference on Human-computer Interaction with Mobile Devices and Services*, ser. MobileHCI '12, 2012, pp. 11–20.

[24] Wikipedia, "Samsung galaxy s series," 2014. [Online]. Available: http://en.wikipedia.org/wiki/Samsung_Galaxy_S_series

[25] C. C. Wu, J. C. Sturm, R. A. Register, and M. E. Thompson, "Integrated threecolor organic lightemitting devices," *Applied Physics Letters*, vol. 69, no. 21, pp. 3117–3119, 1996.

[26] Z. Wang, A. C. Bovik, H. R. Sheikh, and E. P. Simoncelli, "The ssim index for image quality assessment," 2004. [Online]. Available: http://ece.uwaterloo.ca/~z70wang/research/ssim/

[27] ——, "Image quality assessment: From error visibility to structural similarity," *IEEE Trans. on Image Processing*, vol. 13, no. 4, pp. 600–612, Apr. 2004.

[28] S. Iyer, L. Luo, R. Mayo, and P. Ranganathan, "Energy-adaptive display system designs for future mobile environments," in *Proc. of the 1st International Conference on Mobile Systems, Applications and Services*, ser. MobiSys '03, 2003, pp. 245–258.

[29] V. Moshnyaga and E. Morikawa, "Lcd display energy reduction by user monitoring," in *Proc. of Computer Design: VLSI in Computers and Processors*, ser. ICCD '05, Oct 2005, pp. 94–97.

[30] A. Iranli, W. Lee, and M. Pedram, "Backlight dimming in power-aware mobile displays," in *Proc. of the 43rd Design Automation Conference*, ser. DAC '06, 2006, pp. 604–607.

[31] R. Mantiuk, S. Daly, and L. Kerofsky, "Display adaptive tone mapping," *ACM Trans. on Graphics*, vol. 27, no. 3, pp. 68:1–68:10, Aug 2008.

[32] S. H. Kim and J. Allebach, "Impact of hvs models on model-based hlftoning," *IEEE Trans on Image Processing*, vol. 11, no. 3, pp. 258–269, Mar. 2002.

[33] B. Yang, L. Lei, and J. Yang, "Hvs-based structural image quality assessment model," in *Proc of the 7th World Congress on Intelligent Control and Automation*, ser. WCICA '08, Jun. 2008, pp. 8497–8500.

[34] J. Y. Kim and K. C. Choi, "Improvement in outcoupling efficiency and image blur of organic light-emitting diodes by using imprinted microlens arrays," *Display Technology*, vol. 7, no. 7, pp. 377–381, Jul. 2011.

[35] Z. Cao, B. Foo, L. He, and M. van der Schaar, "Optimality and improvement of dynamic voltage scaling algorithms for multimedia applications," *IEEE Trans on Circuits and Systems I: Regular Papers*, vol. 57, no. 3, pp. 681–690, Mar. 2010.

[36] T. I. Corporation, "Tps61060/61/62: Single-wire digital brightness control," *Product Data*, 2004.

[37] A. G. Hauptmann, R. Yan, Y. Qi, R. J. Jin, M. G. Christel, M. Derthick, M.-y. Chen, R. V. Baron, W.-H. Lin, and T. D. Ng, "Video classification and retrieval with the informedia digital video library system," in *Proc. of Text REtrieval Conference*, ser. TREC '02, Nov. 2002, pp. 1–9.

[38] D. Brezeale and D. Cook, "Automatic video classification: A survey of the literature," *IEEE Trans. on Systems, Man, and Cybernetics, Part C: Applications and Reviews*, vol. 38, no. 3, pp. 416–430, May 2008.

[39] J. Li, A. Najmi, and R. Gray, "Image classification by a two dimensional hidden markov model," in *Proc. of International Conference on Acoustics, Speech, and Signal Processing*, vol. 6, Mar. 1999, pp. 3313–3316.

[40] J. Bobulski, "Hidden markov models for two-dimensional data," in *Proc. of the 8th International Conference on Computer Recognition Systems*, ser. CORES 2013, vol. 226, 2013, pp. 141–149.

[41] J. Huang, Z. Liu, Y. Wang, Y. Chen, and E. Wong, "Integration of multimodal features for video scene classification based on hmm," in *Proc. of 3rd Workshop on Multimedia Signal Processing*, Mar. 1999, pp. 53–58.

[42] N. Dimitrova, L. Agnihotri, and G. Wei, "Video classification based on hmm using text and faces," in *Proc. of European Signal Processing Conference*, 2000.

[43] W. Xiong and J. C.-M. Lee, "Efficient scene change detection and camera motion annotation for video classification," *Computer Vision and Image Understanding*, vol. 71, no. 2, pp. 166–181, 1998.

[44] B. T. Truong and C. Dorai, "Automatic genre identification for content-based video categorization," in *Proc. of 15th International Conference on Pattern Recognition*, vol. 4, Sep 2000, pp. 230–233.

[45] B. C. Choi, S. W. Han, B. H. Chung, and J. Ryou, "Design and performance evaluation of temporal motion and color energy features for objectionable video classification," in *Proc. of the 6th International Conference on Advanced Information Management and Service*, ser. IMS '10, Nov 2010, pp. 37–41.

[46] W. Zhou, A. Vellaikal, and C. C. J. Kuo, "Rule-based video classification system for basketball video indexing," in *Proc. of the 2000 ACM Workshops on Multimedia*, ser. MULTIMEDIA '00, 2000, pp. 213–216.

[47] X. Chen, J. Zeng, Y. Chen, M. Zhao, and C. Xue, "Quality-retaining oled dynamic voltage scaling for video streaming applications on mobile devices," in *Proc. of the 49th Design Automation Conference*, ser. DAC '12, Jun. 2012, pp. 1000–1005.

[48] F. Drago, K. Myszkowski, T. Annen, and N. Chiba, "Adaptive logarithmic mapping for displaying high contrast scenes," in *Proc. of Computer Graphics Forum*, vol. 22, 2003, pp. 419–426.

[49] K. W. Tan and et al., "FOCUS: A Usable & Effective Approach to OLED Display Power Management," in *Proc. of UbiComp '13*, Sep. 2013, pp. 573–582.

[50] C. H. Lin and et al., "Catch your attention: Quality-retaining Power Saving on Mobile OLED Displays," in *Proc. of DAC '14*, Jun. 2014, pp. 1–6.

[51] Y. O. Nam and et al., "Power-Constrained Contrast Enhancement Algorithm Using Multiscale Retinex for OLED Display," *Image Processing, IEEE Trans. on*, vol. 23, no. 8, pp. 3308–3320, Aug. 2014.

[52] S. S. Agaian and et al., "Transform-Based Image Enhancement Algorithms with Performance Measure," *Image Processing, IEEE Trans. on*, vol. 10, no. 3, pp. 367–382, Mar. 2001.

[53] B. Anand, K. Thirugnanam, J. Sebastian, P. G. Kannan, A. L. Ananda, M. C. Chan, and R. K. Balan, "Adaptive display power management for mobile games," in *Proc. of the 9th International Conference on Mobile Systems, Applications, and Services*, ser. MobiSys '11, 2011, pp. 57–70.